



HAL
open science

Exceptional Scarp Preservation in SW Namibia Reveals Geological Controls on Large Magnitude Intraplate Seismicity in Southern Africa

R A Muir, B A Whitehead, T New, V Stevens, P H Macey, C A Groenewald, G Salomon, B Kahle, James Hollingsworth, R A Sloan

► To cite this version:

R A Muir, B A Whitehead, T New, V Stevens, P H Macey, et al.. Exceptional Scarp Preservation in SW Namibia Reveals Geological Controls on Large Magnitude Intraplate Seismicity in Southern Africa. *Tectonics*, 2023, 42 (4), pp.e2022TC007693. 10.1029/2022tc007693 . hal-04309176

HAL Id: hal-04309176

<https://hal.science/hal-04309176>

Submitted on 27 Nov 2023

HAL is a multi-disciplinary open access archive for the deposit and dissemination of scientific research documents, whether they are published or not. The documents may come from teaching and research institutions in France or abroad, or from public or private research centers.







L'archive ouverte pluridisciplinaire **HAL**, est destinée au dépôt et à la diffusion de documents scientifiques de niveau recherche, publiés ou non, émanant des établissements d'enseignement et de recherche français ou étrangers, des laboratoires publics ou privés.

Exceptional Scarp Preservation in SW Namibia Reveals Geological Controls on Large Magnitude Intraplate Seismicity in Southern Africa



Key Points:

- Four major neotectonic normal faults are identified in a small area of SW Namibia
- Scarps show evidence of repeated brittle reactivation of ancient ductile structures in large earthquakes
- Exceptional preservation may be responsible for the unexpected density of observable paleoseismic ruptures in the area

R. A. Muir^{1,2} , B. A. Whitehead¹, T. New¹, V. Stevens¹ , P. H. Macey^{1,3}, C. A. Groenewald³ , G. Salomon¹ , B. Kahle^{1,4}, J. Hollingsworth⁵ , and R. A. Sloan¹ 

¹Department of Geological Sciences, University of Cape Town, Rondebosch, South Africa, ²Geology Department, University of the Free State, Park West, South Africa, ³Council for Geoscience, Bellville, South Africa, ⁴Department of Earth and Environmental Sciences, Ludwig-Maximilians-Universität München, Munich, Germany, ⁵Université Grenoble Alpes, Université Savoie Mont Blanc, CNRS, IRD, Université Gustave Eiffel, ISTERre, Grenoble, France

Supporting Information:

Supporting Information may be found in the online version of this article.

Correspondence to:

R. A. Sloan,
alastair.sloan@uct.ac.za

Citation:

Muir, R. A., Whitehead, B., New, T., Stevens, V., Macey, P. H., Groenewald, C. A., et al. (2023). Exceptional scarp preservation in SW Namibia reveals geological controls on large magnitude intraplate seismicity in southern Africa. *Tectonics*, 42, e2022TC007693. <https://doi.org/10.1029/2022TC007693>

Received 6 DEC 2022
Accepted 13 MAR 2023

Author Contributions:

Conceptualization: R. A. Muir, V. Stevens, P. H. Macey, C. A. Groenewald, G. Salomon, B. Kahle, R. A. Sloan
Data curation: R. A. Sloan
Formal analysis: B. A. Whitehead
Funding acquisition: R. A. Sloan
Investigation: B. A. Whitehead, T. New, V. Stevens, C. A. Groenewald, G. Salomon, B. Kahle, R. A. Sloan
Methodology: R. A. Muir, R. A. Sloan
Project Administration: P. H. Macey, J. Hollingsworth, R. A. Sloan
Supervision: R. A. Muir, P. H. Macey, B. Kahle, J. Hollingsworth, R. A. Sloan

Abstract Four previously unrecognized neotectonic fault scarps in southwest Namibia are described. These relatively straight, simple but segmented structures are 16–80 km long and have measured vertical separations of 0.7–10.2 m. We estimate that each is capable of producing earthquakes of M_w 6.4 or greater, indicating that large earthquakes may occur despite limited cumulative displacement. There is strong evidence that some of these scarps were formed by repeated earthquakes. Comparison with aeromagnetic and geological maps reveal that the normal faults reactivate major crustal weaknesses that are orientated north-south and northwest-southeast and perpendicular to the local gravitational potential energy gradient. The presence of these structures in an area with a limited record of instrumental seismicity suggests that the M_{max} of this region may be much larger than generally assumed. They highlight the necessity of incorporating information from fault studies into probabilistic seismic hazard assessments in this region, in a similar way to other stable continental regions such as Australia. The fact that such major structures have gone hitherto unrecorded suggests significant further research is needed to characterize these sources of hazard. The identification of an apparent cluster of large magnitude neotectonic earthquakes in the area may be related to the exceptional preservation potential of scarps rather than indicating an area of comparatively rapid deformation. If this interpretation is correct, then these scarps represent an important indication of the potential seismic hazard across the region, and the occurrence of infrequent large-magnitude seismicity on similar structures should be considered throughout southwestern Africa.

Plain Language Summary Namibia is considered to be a region that has very few large earthquakes. This is partly because previously evidence has not been found in the landscape to suggest that many large earthquakes have occurred in the past. However, in this study we show evidence in SW Namibia of four previously unidentified but significant fault scarps (steps in the landscape generated by movement during earthquakes). These features indicate that significant earthquakes can and have occurred in southern Namibia in the geologically recent past. We also find evidence for repeated motion along these faults and therefore repeated earthquake generation. The extremely dry climate and abundance of hard, well-cemented sediments in the Namib Desert makes it one of the best places in the world for preserving fault scarps. This means we can get a much better idea of the type of earthquakes which could occur over relatively long timescales, and we find evidence for much larger events than would previously have been expected in this area. It is important to consider these features in earthquake hazard assessments in southwestern Africa and other similar areas around the world.

1. Introduction

Namibia (and SW Africa in general) is considered to be a stable continental region (SCR) with little history of significant earthquakes. Within Namibia, instrumentally recorded earthquakes are restricted to smaller than M_w 5.5 (ISC, 2022, Figure 1). Earthquakes recorded in international catalogs reveal a band of seismicity along the west coast within the Namaqua-Natal and Damara belts (Figure 1a, inset). In contrast, the region underlain by the Proto-Kalahari craton appears largely aseismic. Limited network coverage prevents the confident identification of clusters of microseismicity and long-term Global Positioning System (GPS) constraints on strain rates are also

Validation: R. A. Muir, V. Stevens, P. H. Macey, C. A. Groenewald, B. Kahle, R. A. Sloan

Visualization: R. A. Muir, B. A. Whitehead, T. New, B. Kahle

Writing – original draft: R. A. Muir, B. A. Whitehead, T. New, R. A. Sloan

Writing – review & editing: T. New, V. Stevens, P. H. Macey, G. Salomon, B. Kahle, J. Hollingsworth, R. A. Sloan

not available. In this context, paleoseismic studies have the potential to provide information about the tectonics of the region and to inform seismic hazard assessments.

Scarps in southern Namibia can be preserved for unusually extended periods due to exceptionally slow erosion rates (Bierman & Caffee, 2001; Cockburn et al., 2000), an abundance of Cenozoic sediments and sedimentary rocks that are consolidated and strengthened by secondary carbonate cements, and the >30 million year persistence of a semi-to hyper-arid climate in the Namib Desert (e.g., Ward et al., 1983). Consequently, SW Namibia is an exceptional natural laboratory for studying infrequent large-magnitude seismicity in a very slowly deforming region. Understanding the seismic history of such regions is critical for formulating evidence-based seismic hazard assessments. Additionally, the number of well-studied large SCR earthquakes is naturally small compared with earthquakes in plate boundary zones and fundamental questions related to SCR earthquakes remain unanswered (Calais et al., 2016). Evidence of large ruptures in SCRs therefore add important data points to the global data set.

Australia is another region where very low strain rates, occasional large magnitude earthquakes and a fairly sparse national network of seismometers pose similar difficulties for seismic hazard estimation. Apparent discrepancies between the distribution of hazard from the instrumental seismic catalog and the distribution of paleoseismic fault ruptures led to the 2018 probabilistic seismic hazard reevaluation incorporating fault source models into their seismic hazard models for the first time (Allen et al., 2018, 2020; Clark et al., 2016). Such an approach may be necessary in southern Africa as well. At present the catalog of known paleoseismic fault ruptures, and knowledge of important parameters such as slip-rate, remain very limited.

It has been suggested, based on studies in areas such as southern Africa, India, the Eastern US and Australia, that the occurrence of large earthquakes in such regions are controlled by qualitatively different processes to those in more rapidly deforming regions (Calais et al., 2016). This debate focuses on whether large earthquakes are likely to occur on identifiable faults, which repeatedly accumulate and release elastic strain in an analogous manner to more active regions, or if the hazard is instead controlled by a large network of faults which may have been inactive for millions of years, but which are all critically stressed due to very gradual pervasive strain transfer. In this model, events may often be triggered by temporary stress fluctuations associated with, for example, the hydrological cycle or another nearby earthquake, leading to the clustering and migration of seismicity. Once a large earthquake has occurred on an individual fault, this model would suggest that it would only reload very slowly, potentially on Ma timescales, and the current hazard would then be more likely to be focused on other structures which may show little or no sign of previous neotectonic rupture.

The Hebron Fault scarp is the only paleoseismic fault scarp to have been described in detail in Namibia (G. Salomon et al., 2022; Viola et al., 2005; White et al., 2009;). This pure normal-faulting scarp has a length of 45 km, a maximum cumulative offset of 10.1 m and a mean cumulative offset of 5.9 m (G. Salomon et al., 2022). The scarp cuts through alluvial fan calcrete, pedogenic carbonate-cemented sediments that commonly form in near-surface conditions in arid and semi-arid regions (Birkeland, 1984). As a result, the scarp is preserved as a sharp sub-vertical feature for much of its length (G. Salomon et al., 2022; White et al., 2009). A detailed geomorphological study found no direct evidence of a multiple event origin. It remains an open question as to whether this scarp formed in one or more events. Scaling relationships from SCRs (Leonard, 2014) suggest that it likely formed in a small number (1–5) of significant ($\sim M_w 7$) events (G. Salomon et al., 2022). G. Salomon et al. (2022) also concluded that the Hebron Fault followed a pre-existing Mesoproterozoic shear zone and is segmented where a granite batholith interrupts its fabric.

Additional evidence of neotectonics in southern Namibia is scarce. The Dreylingen Fault SW of the Hebron Fault (Figure 1a) is suggested to have recently been active (Viola et al., 2005), yet the fault is mainly expressed in basement rocks and no evidence of the displacement of Quaternary deposits has been presented. A linear array of mud volcanoes off the SW Namibian coast potentially delineate an offshore fault that has been recently active (Viola et al., 2005), however, direct analyses of it are impossible without high resolution seismic data along its length. Finally, Dauteuil et al. (2018) describe micro-scale brittle structures in Cenozoic strata in the coastal regions of the Tsau ||Khaeb National Park (Sperrgebiet) (Figure 1b), which they interpret as evidence of larger neotectonic events. It is however difficult to use cm-scale offsets across small structures to reconstruct regional tectonics.

In NE Namibia, between the Kalahari and the Congo Cratons, Wanke (2005) describes potential displacement of faults within the Eiseb Graben. These faults displace linear dunes thought to have stabilized between 35 and 28 ka indicating that they have been active in the late Quaternary. The Eiseb Graben faults form the western extension

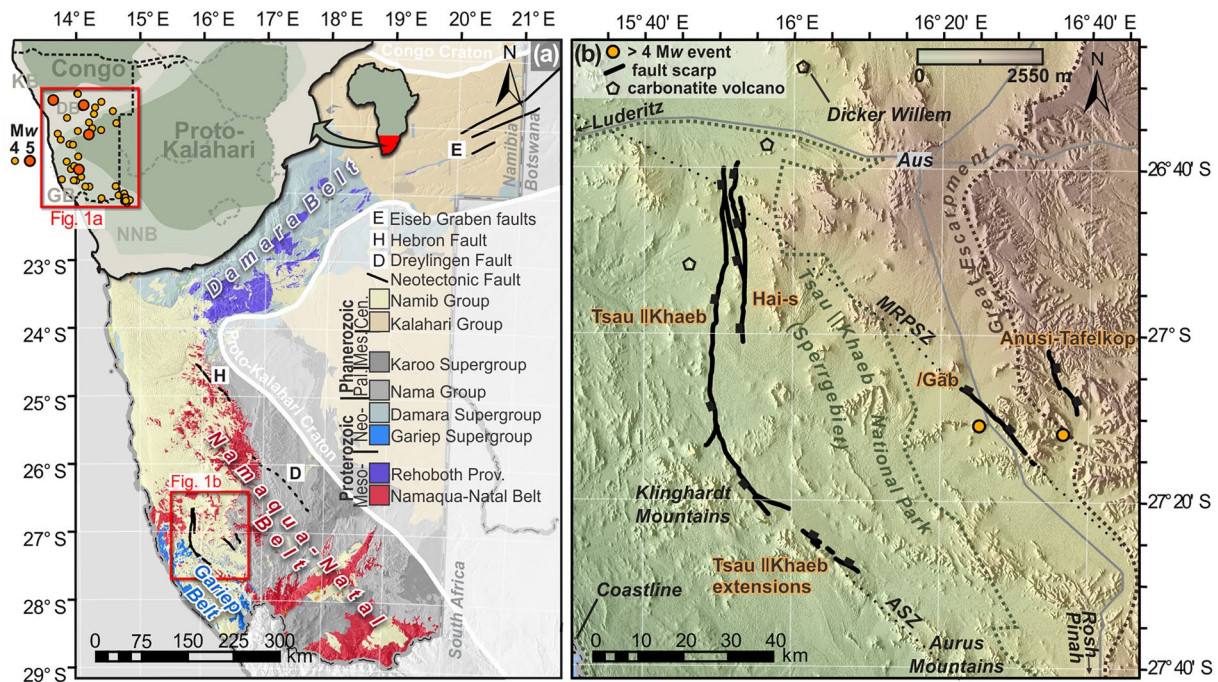


Figure 1. Location and geological setting of newly identified faults. (a) Simplified geology of Namibia. Solid black lines are confirmed neotectonic faults; recent reactivation of the Dreylingen Fault (black dashed line) is speculative. Inset: Country borders; Congo and Proto-Kalahari Cratons; Major orogenic belts of southern Africa; Earthquakes with $M_w \geq 4$ from the International Seismological Centre (ISC) catalog for the period 1964 to July 2022. ASZ—Aurus Shear Zone, DB—Damara Belt, GB—Gariep Belt, KB—Kaoko Belt, MRPSZ—Marshall Rocks-Pofadder Shear Zone, NNB - Namaqua-Natal Belt. (b) Digital Elevation Model (NASA:JPL, 2013) and newly identified fault scarps near Aus, southern Namibia, between the coast and the Great Escarpment within and adjacent to the Tsau I|Khaeb National Park. Roads are shown as gray lines.

of the faulting associated with the Okavango region (the SW branch of the East African Rift) and follow the Pan-African Damara Belt which separates the cratons (Figure 1a). It has been suggested rifting may continue across northern Namibia to link with NNW-SSE striking faults in the Namibian Highlands or continue to the Mid-Atlantic Ridge via the Walvis Ridge (Daly et al., 2020; Wedmore et al., 2021), although these interpretations remain hypotheses due to the limited constraints on rifting from geodesy, seismology and geomorphology within Namibia (Hasterok et al., 2022).

Here, we present remote sensing and field evidence for four newly identified fault scarps in southern Namibia, which have significant implications for regional seismic hazard and contribute to the international catalog of SCR events. We demonstrate that this faulting reactivates (and in some cases terminates against) pre-existing shear zones, indicating that the older structures control seismic hazard in the region.

2. Geological and Geomorphological Setting

The geology of southern Namibia records repeated deformation events during the Proterozoic, Cambrian, Carboniferous–Jurassic and Cretaceous. The resulting crust along and outward of the western margin of the Proto-Kalahari Craton (Figure 1) contains a complex set of structures with varying orientations (Corner & Durrheim, 2018). We argue that these structures determine the location and orientation of neotectonic faulting, and affect the potential size of earthquakes and the scaling relationships observed for these faults. A number of studies have established that pre-existing shear zones play an important role in controlling the location and orientation of African rifts and, more recently, individual earthquake ruptures (e.g., Daly, 1988; Kolawole et al., 2018; Wedmore et al., 2022). Consequently, we now briefly review the orientations and ages of large-scale fabrics and structures generated during the significant tectonic episodes that have affected the study area.

1. *Mesoproterozoic, generally NW-SE trending*, penetrative, gneissic foliation developed during multiple phases of folding and thrusting in the Namaqua Orogeny, during the assembly of southern Rodinia (Johansson et al., 2022; Macey et al., 2022). This foliation broadly aligns with subvertical NW-SE trending transpressional

- shear zones, such as the Marshall Rocks-Pofadder Shear Zone (MRPSZ), that formed at the end of the orogenic cycle.
2. *Neoproterozoic (Tonian), North-South to NNW-SSE orientated*, extensional brittle structures that formed during the emplacement of the *syn-rift* Gannakouriep dyke swarm and associated East-West rifting and formation of the Gariiep Basin and intrusive complexes (Reid et al., 1991; Rioux et al., 2010).
 3. *Neoproterozoic (Ediacaran) to early Cambrian NW-SE trending*, transpressive Gariiep Belt ductile structures, for example, the Aurus Shear Zone in the study area, which formed during the assembly of Gondwana (Frimmel, 2008; Thomas et al., 2016). Other pre-existing NW-SE structures, for example, the MRPSZ were also reactivated; Concurrently, NW-SE compression in the Damara Belt, central Namibia, resulted in a NE-SW tectonic fabric there that is roughly orthogonal to the Namaqua-Natal Belt and Gariiep Belt structures further south. During this compressional regime, a foreland basin developed, into which the Nama Group was deposited. Today, the Nama Group outcrops widely at the top of the escarpment and plateau in southern Namibia and overlies igneous and metamorphic units with a regionally map-able nonconformity.
 4. *Post-Nama Group, predominantly N-S and NW-SE trending*, extensional faults of speculative age that are evident in satellite imagery as lineaments on the modern-day escarpment and plateau (see G. Salomon et al., 2022; Viola et al., 2005, for further details).
 5. *Carboniferous to Jurassic NE-SW orientated*, basin-bounding extensional faults that accommodate hundreds of meters of Karoo Supergroup sedimentary strata (M. M. Johnson et al., 1996).
 6. *Early Cretaceous, coast-parallel ~N-S normal faults* that accompanied the opening of the South Atlantic and basaltic volcanism during the rifting of SW Gondwana (E. Salomon et al., 2015; Reid & Rex, 1994; Torsvik & Cocks, 2013), that ultimately resulted in the late Mesozoic–present-day passive margin. Minor alkaline intrusions also occurred in the Early Cretaceous in the coastal region of the Tsau ||Khaeb National Park (Marsh, 1975).
 7. *Paleogene volcanism* occurred in the Tsau ||Khaeb National Park in the Klinghart Mountains (Marsh et al., 2010) and along a NE-SW trending line (Corner, 2000; Walter et al., 2022). The nature and tectonic framework of these volcanic events are poorly understood (Walter et al., 2022).

Following the significant km-scale accelerated Cretaceous erosion during and post-dating Gondwana breakup revealed through low temperature thermochronometry (Brown et al., 1990; Raab et al., 2005; Wildman et al., 2021), southern Namibia entered a prolonged phase of relative tectonic quiescence, landscape stability, and slow erosion rates, evidenced by the presence of ancient (estimated up to 40 Ma) erosional land-surfaces (Picart et al., 2020) and cosmogenic nuclide measurements that indicate an erosion rate of, for example, 8 m/Myrs (Bierman & Caffee, 2001; Cockburn et al., 2000).

2.1. Age of Fault Scarps

The exceptional landscape stability in southern Namibia is due to the predominantly stable continental setting it occupies, but also the prolonged aridity of the Namib Desert. The aeolian and subordinate fluvial desert sediments record aridity since at least 30 Ma and hyper-arid conditions for the last 15 Myrs (Dingle et al., 1983; Miller et al., 2021; Ward et al., 1983). Much of these sediments are consolidated by secondary carbonate cements (forming calcrete) which are of speculative genesis and age and occur widely in southern Namibia including the Hebron Fault scarp (G. Salomon et al., 2022; White et al., 2009) and in the vicinity of the fault scarps described in this study.

Pickford (2015) points out that most of the surface moisture in the coastal Sperrgebiet is supplied from fog that is blown inland and therefore prefers the term “calc-crust” to describe these cemented units. While Pickford (2015) is correct in emphasizing the role of fog in generating near-surface moisture in the Namib, we do not differentiate between these two genetic classifications in this study. It seems probable that near-surface moisture was supplied through multiple sources with ocean-derived fog likely a large contributor near to the coast but with a diminishing role progressively inland.

During our fieldwork in the Namib, within the inland regions of the Tsau ||Khaeb National Park and at the base of the Great Escarpment (Figure 1), we observed abundant near-surface carbonate-cemented sediments that are well-exposed in fault scarps and we refer to them throughout this paper simply as calcrete. Some, but not all of these units are possibly the in-land correlatives of calc-crusts described from coastal regions that have been biostratigraphically dated to two long-lived periods in the Middle–Late Miocene (Calc-crust 1), and Pliocene to

Holocene (Calc-crust 2; Pickford, 2015). However, the accuracy of these ages have not been verified by radiometric dating methods, and the isolated outcrops in our study area cannot be confidently correlated to better studied coastal outcrops (e.g., Pickford et al., 2008), reducing their utility in constraining fault scarp age and slip rates. Until radiometric ages are attained for these units and correlations with studied outcrops are made with confidence, we withhold from assigning specific ages to the fault scarps described here. Carbonate-cemented sediments could be anything from Middle–Upper Miocene, the biostratigraphically constrained age of the oldest calcrete (i.e., Calc-crust 1 of Pickford (2015)) to Holocene, with multiple periods of carbonate precipitation likely. Accordingly, the fault scarps studied here may have initiated at any point in the last ~15 Ma, which is compatible with Early Miocene age estimates for the major planation surface that dominates the in-land Tsau || Khaeb National Park and is displaced across the faults (planation surface S6 of Picart et al., 2020).

3. Methods

A geological mapping survey of the area along the Great Escarpment SE of Aus revealed a previously unidentified fault scarp in June 2019. Subsequently, satellite images were used to locate and delineate additional recently active faults that displace sedimentary cover. This was principally performed using Bing Maps and Pléiades imagery in ArcGIS and QGIS. Once lineaments were mapped, the Shuttle Radar Topography Mission NASA-DEM (NASA:JPL, 2013) was used to determine whether a scarp is present along their lengths at the resolution available. Higher, 0.5 m resolution Pléiades satellite imagery along the lengths of the most promising faults were obtained for further assessment of their character. Aeromagnetic intensity maps and 1:50k geological maps were supplied through the Geological Survey of Namibia. Since the majority of the mapped lineaments ran through unconsolidated sediments and calcrete of the Namib Group as well as recent alluvium and scree, they were superimposed over the aeromagnetic maps (intensity reduced to pole) in which major aeromagnetic lineaments were mapped. Following remote sensing, fieldwork was conducted in May 2021 to confirm whether the most promising lineaments mapped were indeed fault scarps. Real-time kinematic (RTK) positioning GPS surveys were carried out along representative portions of four scarps using a TRIMBLE R8 GNSS/R6/5800 GPS base station and hand-held rover mounted to a 2 m high measuring pole. GPS measurements were taken at 2 s intervals as the rover was walked along a pre-determined 200–500 m straight path that was perpendicular to and crossed the fault scarp avoiding local scarp complexities and post-slip sedimentary depositional and erosional modifications.

The displacement D and throw T were derived from these profiles (insets in Figures 2–4). Linear regression was used to fit straight lines through points above and below the scarp. Areas affected by small channels close to the scarp were manually excluded in some cases (e.g., profile A1 Figure 2). The vertical separation V between the projection of these two surfaces was then calculated at the center of the scarp. To convert the vertical separation to the throw in cases where the fault dips in the same direction as the slope the following equation was used:

$$T = \frac{V \cos(\delta) \sin(\alpha)}{\sin(\delta - \alpha)} + V \quad (1)$$

where δ is the fault dip and α is the average of the two slopes (adapted from K. L. Johnson et al., 2018). If the normal fault dips in the opposite direction of the slope,

$$T = \frac{V \cos(\alpha) \sin(\delta)}{\sin(\alpha + \delta)}. \quad (2)$$

Equation 2 was originally intended for use with reverse faults dipping in direction of the slope (adapted from Thompson et al. (2002)), however this equation also applies to normal faults dipping in the opposite direction of the slope. The geometry of both cases is illustrated in Figure S1 in Supporting Information S1. For either scenarios,

$$D = \frac{T}{\sin(\delta)}. \quad (3)$$

We do not have firm constraints on the dip of the faults described here other than the near-surface dip of the Anusi-Tafelkop Fault, which has a polished bedrock scarp with a dip of 73°, although this may not be representative of the dip at seismogenic depths (Figure 6a). Given the steep dip observed at this location, the evidence for the reactivation of steeply dipping ductile shear zones and comparison with the Hebron Fault we assign a dip of

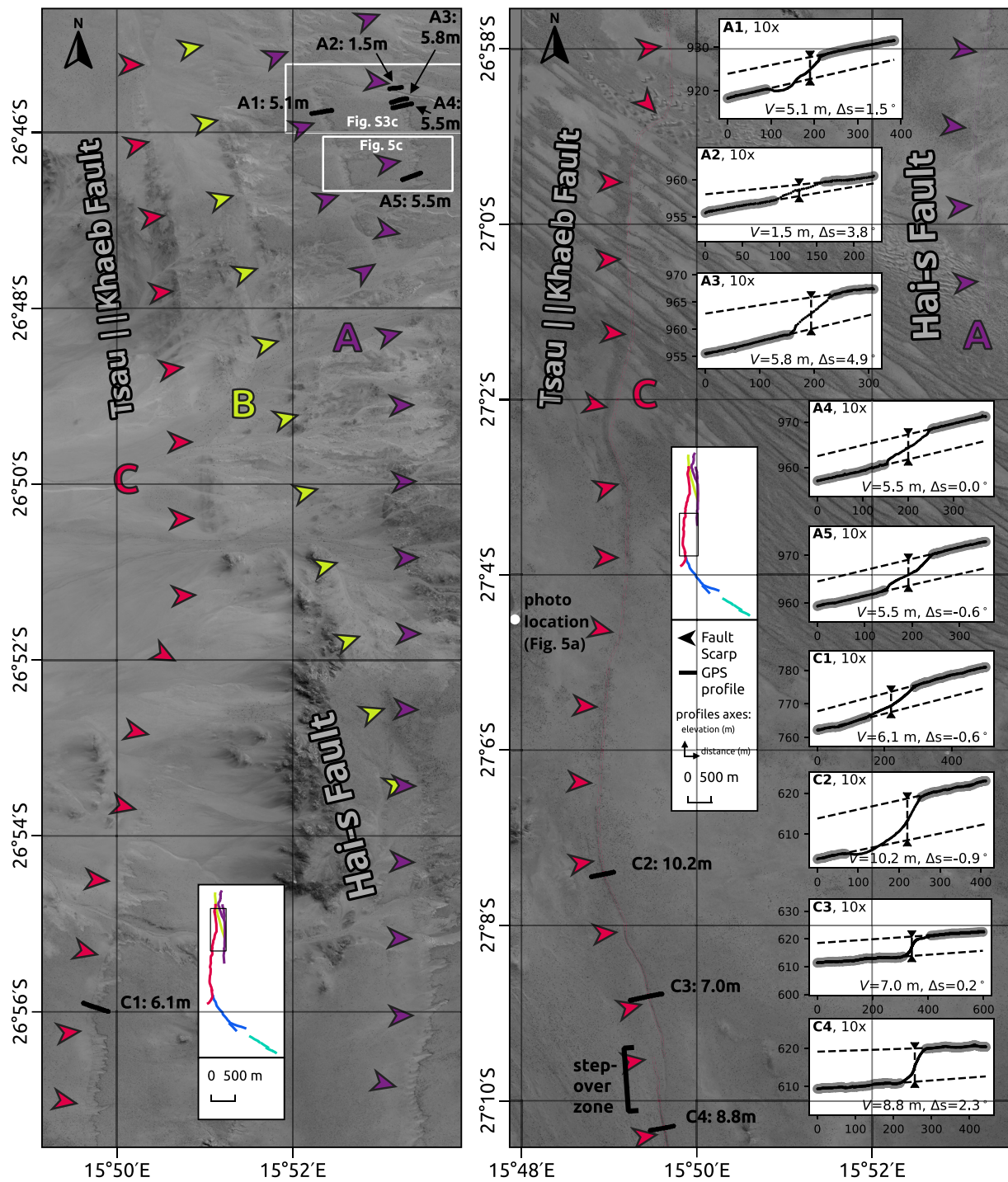


Figure 2. Pléiades imagery of the Hai-s (segments A and B) and Tsau || Khaeb (Segment C) faults, with location of the GPS profiles. Insets show the region of the fault trace that is enlarged and the elevation profiles across the scarp with 10x vertical exaggeration. Colored letters and arrows correspond to fault segments discussed in the text and Tables S1 and S2 in Supporting Information S1. Arrows are positioned on the down-thrown side of the fault. The extent of Figure 5c is shown by the white box. V: vertical offset across the fault; Δs : difference in angle of displaced surfaces.

60° to all of the faults in this study as our preferred value. We include the results for dips of 45° and 75° in Tables S1 and S2 in Supporting Information S1 to illustrate the uncertainty associated with this assumption.

The length of the faults were assessed from measuring the visible surface rupture length (SRL). Two faults were separated into segments based on their geometry, though this should not be taken to imply that these segments

will necessarily fail in separate events or that past events necessarily ruptured an entire segment. The presently observable SRL may be lower than the true length of the fault that has failed. This may be either because the earthquake did not breach the surface across the whole length of the fault, or because the tapered ends of the rupture have been censored by subsequent erosion (e.g., Leonard, 2014; Stirling et al., 2002). A recent compilation of dip-slip (DS) earthquakes in SCR regions suggested that the length could be approximated as the SRL when longer than 15 km (Leonard, 2014). As this is the case for all of the ruptures studied we simply report the SRL and use this as the fault length for calculations and comparisons, but note that this is likely to be an underestimate of the true rupture length.

In order to assess the likely displacement in a single event, and the likely magnitude of individual earthquakes, we use regression-based relationships from DS faults in SCR regions (Leonard, 2014). The expected average displacement D_{av} is calculated from L_m , the length of the rupture in meters:

$$\log D_{av} = a + 0.833 \log(L_m), \quad \text{for } L_m > 2500m \text{ for DS in SCR} \quad (4)$$

where $a_\mu = -3.572$, $a_{-\sigma} = -3.78$ and $a_{+\sigma} = -3.38$ for the mean (μ) and one standard deviation ($\pm\sigma$) results of a partial linear regression. Similarly M_w , the moment magnitude is calculated from L_{km} the length of the rupture in kilometers:

$$M_w = a + 1.667 \log(L_{km}), \quad \text{for } L_{km} > 2.5km \text{ for DS in SCR} \quad (5)$$

where $a_\mu = 4.32$, $a_{-\sigma} = 4.12$ and $a_{+\sigma} = 4.51$. The D_{av} and M_w estimates are given in Table S2 in Supporting Information S1 alongside the segment lengths L and the average observed displacements \bar{D} .

These relationships result in slightly larger offsets and magnitudes than empirical relationships based on datasets dominated by earthquakes in more rapidly deforming regions (e.g., Wells & Coppersmith, 1994). On the other hand, as noted above, it is likely that the fault lengths used may underestimate the true length by a few kilometers resulting in the possible underestimation of these values. In addition, the majority of the events the Leonard (2014) regressions are based on are reverse faults rather than normal faults.

To roughly estimate the range of the number of events that may have formed the scarp (n) we calculate $\frac{\bar{D}}{D_{av}(a_{+\sigma})}$ rounded down to the nearest integer with a minimum value of 1 and $\frac{\bar{D}}{D_{av}(a_{-\sigma})}$ rounded up to the nearest integer. \bar{D} is the average displacement calculated from profiles from that segment or fault. Where younger surfaces showed a dramatic reduction in scarp height compared to neighboring older surfaces (A2 and F2) these were excluded from the average. Due to limited time in the field only a small number of profiles could be measured and so \bar{D} should not be interpreted as a reliable average total displacement along the whole fault and is simply reported here to allow an approximate estimate of the number of scarp-forming events.

4. Results

In the following sections, we describe the newly identified faults in detail. The names of these faults are shown, along with their location, in Figure 1b. Pronunciations of the three Khoekhoegowab names are provided as supplementary audio files.

4.1. Tsau ||Khaeb

The Tsau ||Khaeb and Hai-s faults (Figures 2 and 3) are both situated within the Tsau ||Khaeb National Park (Sperrgebiet) and their surface traces run through predominantly Cenozoic calcretes and elsewhere through unconsolidated, active aeolian and sheet-wash alluvial deposits. The Tsau ||Khaeb scarp (segments C and D in Figure 2) is 80 km long, with an arcuate trace that is ~N-S at its northern extent (26° 40'S) and gradually curves to attain a NW-SE orientation at its southern extremity (27° 20'S). Two short splays are present along its length, there is a small, 200 m wide step-over zone (27° 10'S, Figure 5a) and the fault trace merges with one branch of the Hai-s fault in the north (Figure 1b; 2). The vertical separations measured along the Tsau ||Khaeb Fault scarp ranged from 1.1 to 10.2 m (Figure 2). Further to the SW, the fault trace is not clearly visible in satellite imagery but there are sporadic parallel scarps (Segment E in Figure 3). These are considered extensions to the Tsau ||Khaeb Fault and were not studied in detail.

Segment C, the central N-S orientated portion of the scarp, has higher vertical offsets (from N to S: 6.1, 10.2, 7.0, 8.8 m) than the southern, curved Segment D (1.8, 3.2, 1.1, 3.0 m). Two significant branches occur along the southern portion of the fault at 27° 11'S and 27° 20'S. Both were observed to have small and diffuse scarps in the field (e.g., profile D3). For most of its length, the scarp runs through calcrete that is covered by a thin (<50 cm) veneer of unconsolidated aeolian sand barring a small portion that is covered by an active longitudinal and barchan dune field (Figure 3).

In the northern section of the fault (at profile C1, Figure 2) the scarp has two distinct slope breaks which suggest this is a compound scarp: an older scarp that has retreated backward as a result of post-slip erosion, has a highly irregular trace in map-view and a scree apron; a second younger, steeper and straighter scarp that coincides with the fault trace and perhaps represents the offset in the most recent event. Similar features are observed in two branches of the Hai-s Fault, which are described and interpreted in detail in Section 5.2 (Figures 5c–5e; Figure S3 in Supporting Information S1).

4.2. Hai-s

The Hai-s Fault trace is more complex than the other faults described, with a main axis that runs N-S, parallel to the northern section of the Tsau ||Khaeb Fault and two sub-parallel branches that join it at acute angles (Figure 1b; Segments A and B in Figure 2). The longest of these branches (Segment B) runs sub-parallel to the main fault for 26 km. The total length of the fault is 40 km with total vertical offsets of 5.1–5.8 m in areas where the scarp runs through sediments preserved by well-indurated calcrete. The offset value is suddenly reduced where the fault runs through unconsolidated alluvium in a river bed (profile A2 in Figure 2 and Figure S3 in Supporting Information S1). In this area it has a vertical separation of 1.1 m (Figure 2 profile A2, note the proximity of profiles A3 and A4). As in the northern part of the Tsau ||Khaeb Fault there are two distinctive slope breaks which suggest they are compound scarps (note the steep section at the front of the scarp captured in profiles A3, A4, A5 in Figure 2 and Figure S3 in Supporting Information S1). A similar feature may be visible in A1, but interpretation is less clear due to the presence of a small channel in front of the scarp).

There are two potential interpretations of the multiple slope breaks observed: (a) that they result from differential erosion following a single event; or our preferred explanation (b) that they result from at least two earthquakes, separated by a significant time. The first explanation could be correct if, for example, a resistant lithology was overlain by softer material, for example, bedrock overlain by sediments. In this case, the offset in the resistant lithology could have been preserved as a straight, steep feature whilst the softer overlying layer retreated backwards, due to ease of erosion, from the initial single rupture. However, field observations reveal similar calcretes exposed along both scarps. The straight, frontal scarp also appears to cross alluvium, for example, at A2; here, the observed is directly along-strike of the frontal scarp, is relatively straight and has a similarly small height (~1 m) to that of the frontal scarp. Whilst the height of scarps created in a single earthquake can vary significantly as the rupture crosses from duricrusts to unconsolidated sediments, it is highly unlikely that the scarp in more cemented sediments would retreat further than that in unconsolidated alluvium. The frontal scarp therefore appears to be largely insensitive to lithology and has not retreated appreciably more in unconsolidated alluvium compared to well-cemented duricrusts. Geomorphologically, the frontal scarp is much straighter than the high-sinuosity main scarp (e.g., Figure 5c), also giving the impression that it formed more recently. Finally this frontal scarp has a similar height to that expected for a single event on a fault of this length (Table S2 in Supporting Information S1, Leonard, 2014).

We therefore consider that the complex, multiple scarp morphology results from at least two separate earthquakes. The straight, steep scarp represents the most recent rupture on this fault. The larger, sinuous scarp behind it is then interpreted to have formed in one or more previous earthquakes; its morphology and position result from having more time to erode compared to the frontal scarp.

4.3. Anusi-Tafelkop

The Anusi-Tafelkop Fault runs 15 km across valleys and mountains at the foothills of the Great Escarpment (Figures 1b and 4). The fault trace has a general NNW-SSE trend and has a single step-over zone that separates two segments; this step-over is largely obscured by recently active alluvium (Figure 6a). The scarp has a maximum measured height of 3.2 m, which is preserved in a section along the fault where it displaces

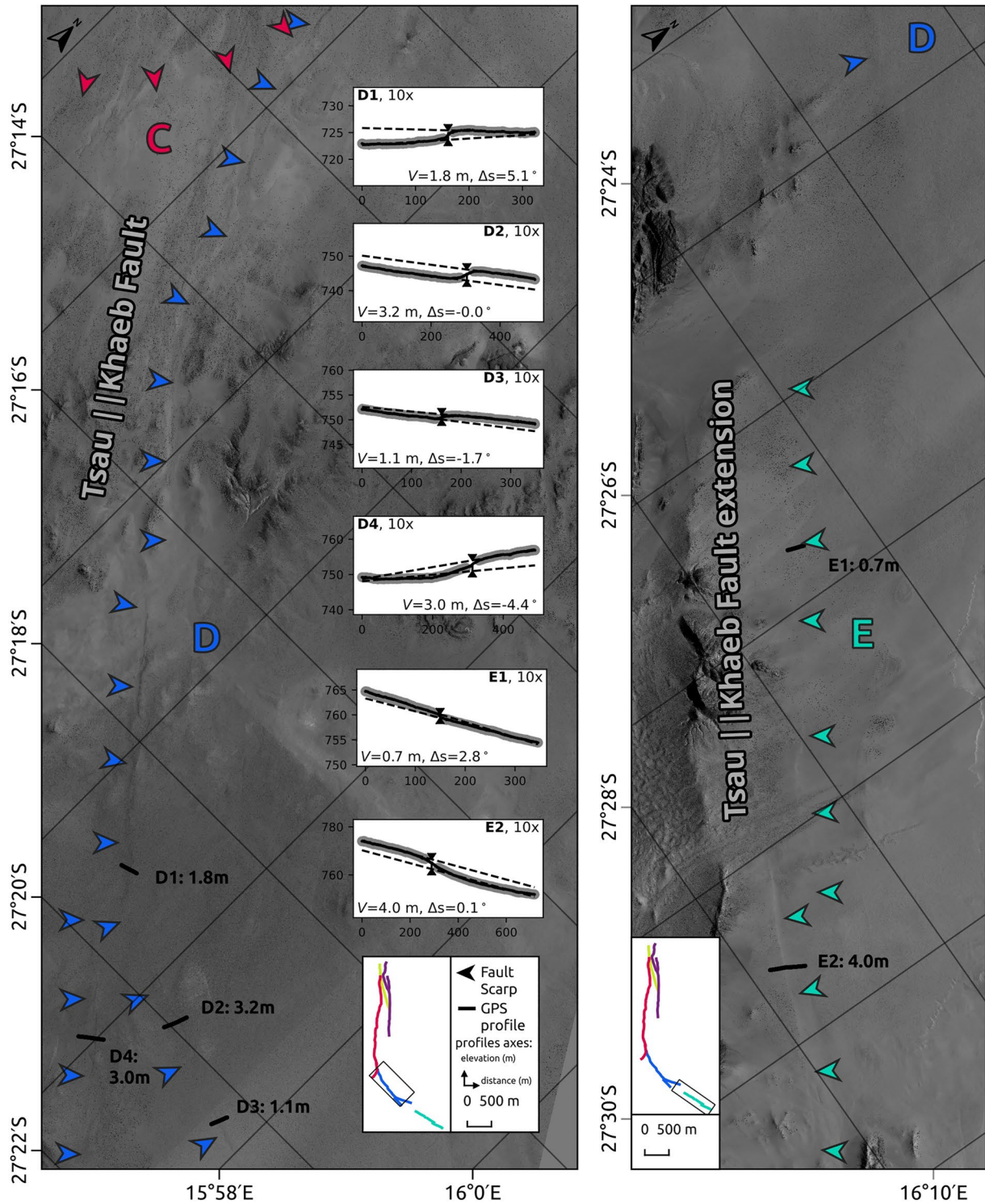


Figure 3. Pléiades imagery of the southern Tsau //Khaeb Fault trace (segments C and D) and extensions (Segment E) with location of the GPS profiles. Insets show the region of the fault trace that is enlarged and the elevation profiles across the scarp with 10× vertical exaggeration. Colored letters and arrows correspond to fault segments discussed in the text and Tables S1 and S2 in Supporting Information S1. Arrows are positioned on the down-thrown side of the fault. Abbreviations as in Figure 2.

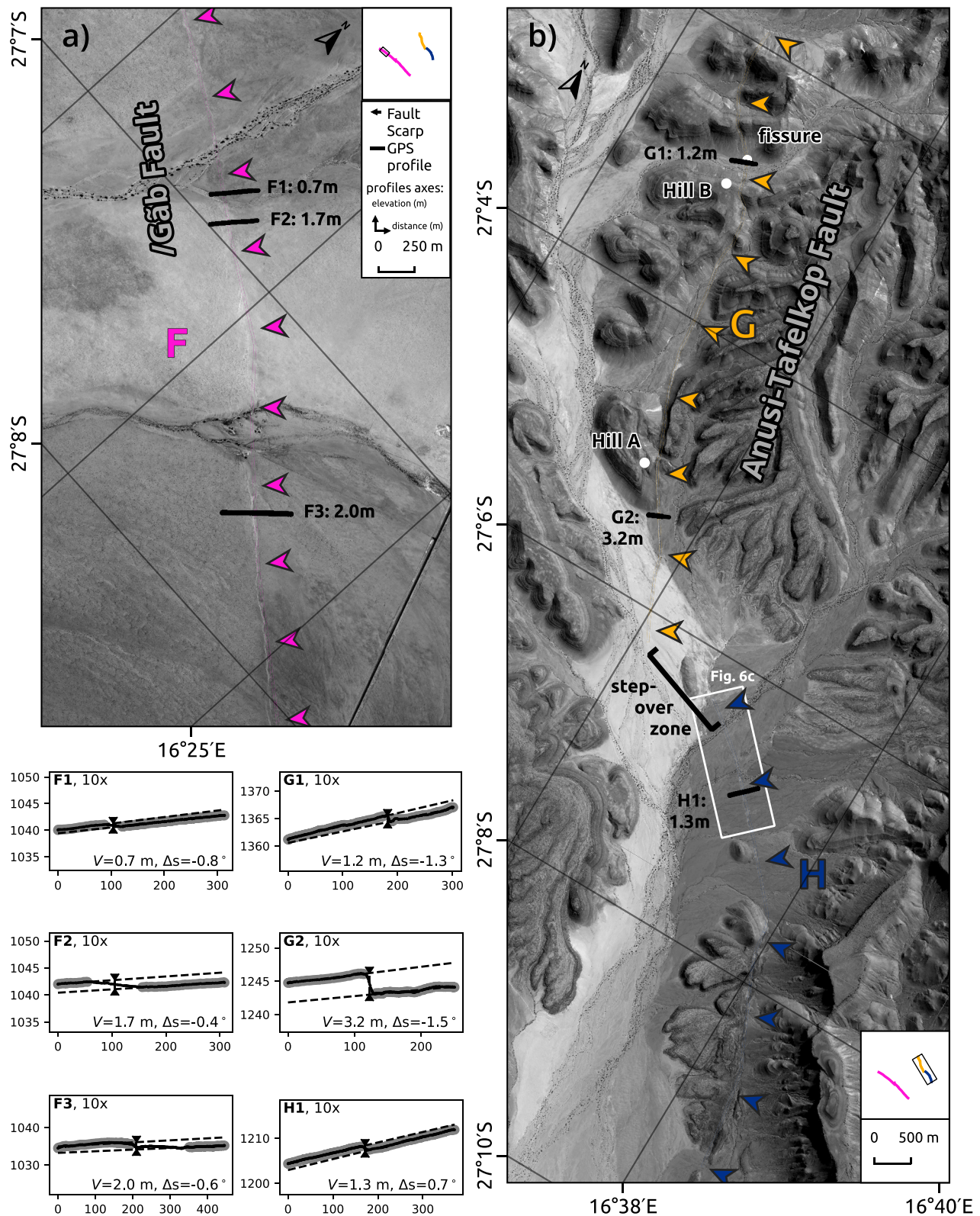


Figure 4. Pléiades imagery of the (a) /Gâb Fault and the (b) Anusi-Tafelkop Fault, with location of the GPS profiles. Hill A, Hill B, and the fissure are discussed in the text and displayed in Figure S2a and S2b in Supporting Information S1. Insets show the region of the fault trace that is enlarged and the elevation profiles across the scarp with 10x vertical exaggeration are positioned at the bottom left. Colored letters and arrows correspond to fault segments discussed in the text and Tables S1 and S2 in Supporting Information S1. Arrows are positioned on the down-thrown side of the fault. The extent of Figure 6c is given in white. Abbreviations as in Figure 2.

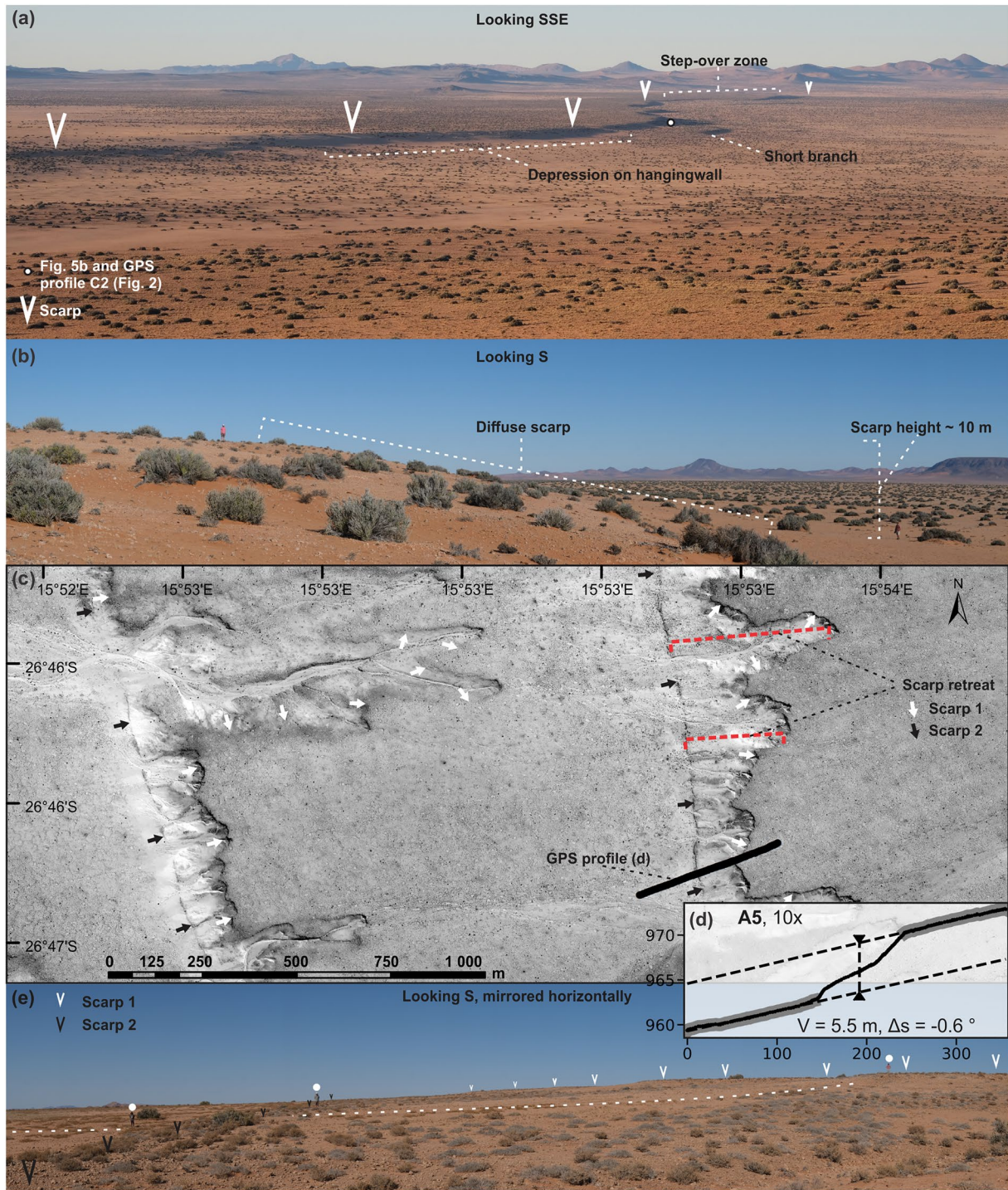


Figure 5. Morphology of surface rupture scarps. (a) Tsau ||Khaeb Fault scarp at sunrise casting a shadow onto the hanging wall. The maximum vertical offset along this portion of the fault is 10.2 m. See Figure 2 for photograph location. (b) 10 m high diffuse scarp along the Tsau ||Khaeb Fault. (c) Pléiades imagery of compound scarps along each of two branches of the Hai-s Fault indicating multiple events and post-slip scarp retreat (see Figure 2 for location). (d) GPS data along the profile indicated in (c), showing two distinct scarps. (e) A diffuse, higher, older, eroded scarp (labeled Scarp 1 in c) and a steeper, younger scarp (labeled Scarp 2 in c) with offset surfaces indicated with dashed lines. White circles highlight the position of people for scale. See Figure S3 in Supporting Information S1 for additional photographs and the precise camera location used to document these scarps.

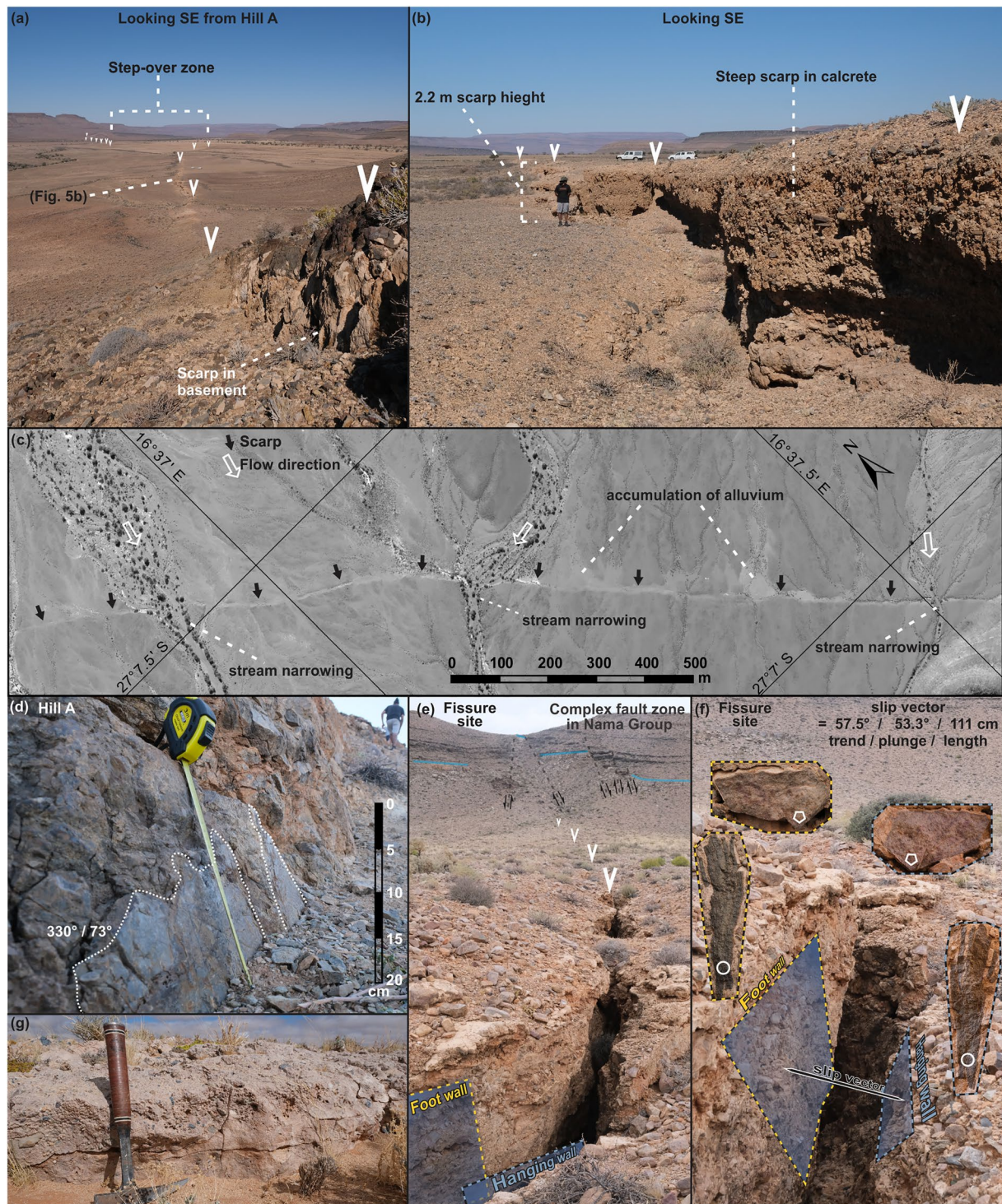


Figure 6. Morphology of fault scarps. See Figure 4 for locations. (a) Anusi-Tafelkop Fault scarp offsetting basement rocks and alluvial sediments in a broad, 7 km wide river valley. View toward the SW. (b) Vertical scarp preserved in a thick (>2.2 m) calcrete. (c) Pliades imagery of a section of the Anusi-Tafelkop Fault scarp where stream incision and sediment accumulation is affected by the fault. Black arrows are on the down-thrown side of the scarp. (d) Polished plane at the Anusi-Tafelkop Fault scarp at Hill A, outlined in white, that is interpreted as the fault plane and has a measured orientation of $330^\circ / 73^\circ$. (e) Fissure along Anusi-Tafelkop Fault and complex fault zone in basement. Blue lines are non-conformity at the base of the Nama Group. (f) Fissure in northern section of the Anusi-Tafelkop Fault that displays individual offset clast fragments within well-indurated calcrete. Slip vector was calculated from averaging four displaced clast fragment pairs. Insets show examples of clast fragment pairs and white shapes are points used to calculate the slip vector. See Figure S4 in Supporting Information S1 for detailed view of the offset clast fragment pairs. (g) Calcrete exposed in the /Gáb Fault scarp at profile F3 that is also typical of the calcretes along the Tsau || Khaeb and Hai-s scarps. In general, these contain fewer, smaller clasts than the calcrete exposed in the Anusi-Tafelkop Fault scarp (see b, e and f).

well-indurated gravel-calcrete immediately south of Hill A (Figure S2a), but is greatly reduced where intersecting unconsolidated alluvium and at the southern termination of segment H (Figures 4 and 6a and 6b). The scarp displaces basement rocks of the Namaqua-Natal Belt and the Nama Group on the flanks and atop Hill A, respectively. Here, where the fault passes through the Nama Group, a polished planar surface is exposed ($330^{\circ}/73^{\circ}$) that we interpret to be the fault plane (Figures 4 and 6a–6d). Further north along the fault (Figure 4; Figure S2b in Supporting Information S1) a narrow fissure within well-indurated calcrete is present (strike = 358°), which exhibits individually displaced clast fragments, of which four pairs were matched and their displacements measured and averaged to give a slip vector with an azimuth of 57.5° ($\sigma = 1.1^{\circ}$), a plunge of 53.3° ($\sigma = 1.8^{\circ}$), and a length of 111 cm ($\sigma = 0.5$ cm) (Figures 6e and 6f; Figure S4 in Supporting Information S1).

4.4. /Gāb

A 21 km long NW-SE orientated fault scarp exists on either side of the C13 road between Aus and Rosh Pinah, which we name the /Gāb Fault (Figure 1b). Measured scarp heights range from 0.7 to 4 m in the displaced calcrete (Figures 4 and 6g). A vertical offset of 0.7 m was measured in profile F1, where a younger unconsolidated alluvium associated with a river channel is displaced. Comparison of profiles F1 and F2 (Figure 4) shows evidence for a sudden change in scarp height across a boundary between older and younger geomorphological surfaces. The higher scarps are also significantly more diffuse, spanning up to 50 m horizontally (Figure 4).

4.5. Throw, Displacement, and Magnitude Estimates

The vertical separations shown in Figures 2–4 and derived estimates of throw and displacement are summarized in Table S1 in Supporting Information S1. These displacements are not necessarily expected to have formed in a single event. Some of the profiles show evidence of compound scarps and abrupt changes of scarp height across adjacent geomorphological surfaces of different ages which strongly suggest multiple events generated them.

These results suggest that many of these scarps formed as a result of multiple events. Offsets in relatively young fluvial sediments along the Hai-s and /Gāb faults (Figures 2 and 4; Table S1 in Supporting Information S1) are consistent with the expected offset from a single event (Table S2 in Supporting Information S1), but the higher scarps on the Hai-s and Tsau ||Khaeb faults (Figures 2 and 3; Table S1 in Supporting Information S1) likely formed in three or more events (Table S2 in Supporting Information S1). Although scaling relationships (Leonard, 2014) suggest that the /Gāb Fault scarp could have formed in a single event if the offset were toward the upper end of the range obtained, the abrupt change in height between surfaces of different ages suggests that it is more likely to have formed in two events (Table S2 in Supporting Information S1).

5. Discussion

Having identified these unexpected earthquake ruptures, we now discuss the implications for understanding SCR earthquakes, the factors controlling their localization, and the consequences for seismic hazard assessment. We argue that the pre-existing structures in the area play an important role in controlling their location and orientation, and that reactivation occurs where such structures are well-oriented with respect to stresses arising from the gradients in gravitational potential energy (GPE). These structures are well-expressed in aeromagnetic data and may be weakened by extensive hydrous retrogression. Such structures could be identified regionally to inform hazard analyses, and the evidence for repeated rupture presented here suggests that they remain ongoing sources of elevated seismic hazard. The fact these earthquakes reactivated well-developed ductile structures has allowed large earthquakes to occur on long, geometrically simple faults despite apparently limited cumulative brittle offset. This makes it very difficult to rule out a large earthquake on ancient predominantly ductile structures which may not be viewed as a potential source of hazard. The instrumental record appears to support increased activity along the western margin of the craton and along the edge of the Great Escarpment but events are not clustered within the vicinity of these scarps. The apparent cluster of large-magnitude paleoearthquakes may be caused by preservation bias rather than representing a localized region of elevated seismic hazard. The paleoearthquakes described here are likely to have greatly exceeded the maximum observed instrumental magnitude and highlight the dangers of over-reliance on instrumental catalogs for seismic hazard analysis in the region and suggest greater incorporation of paleoseismology and geological constraints is necessary.

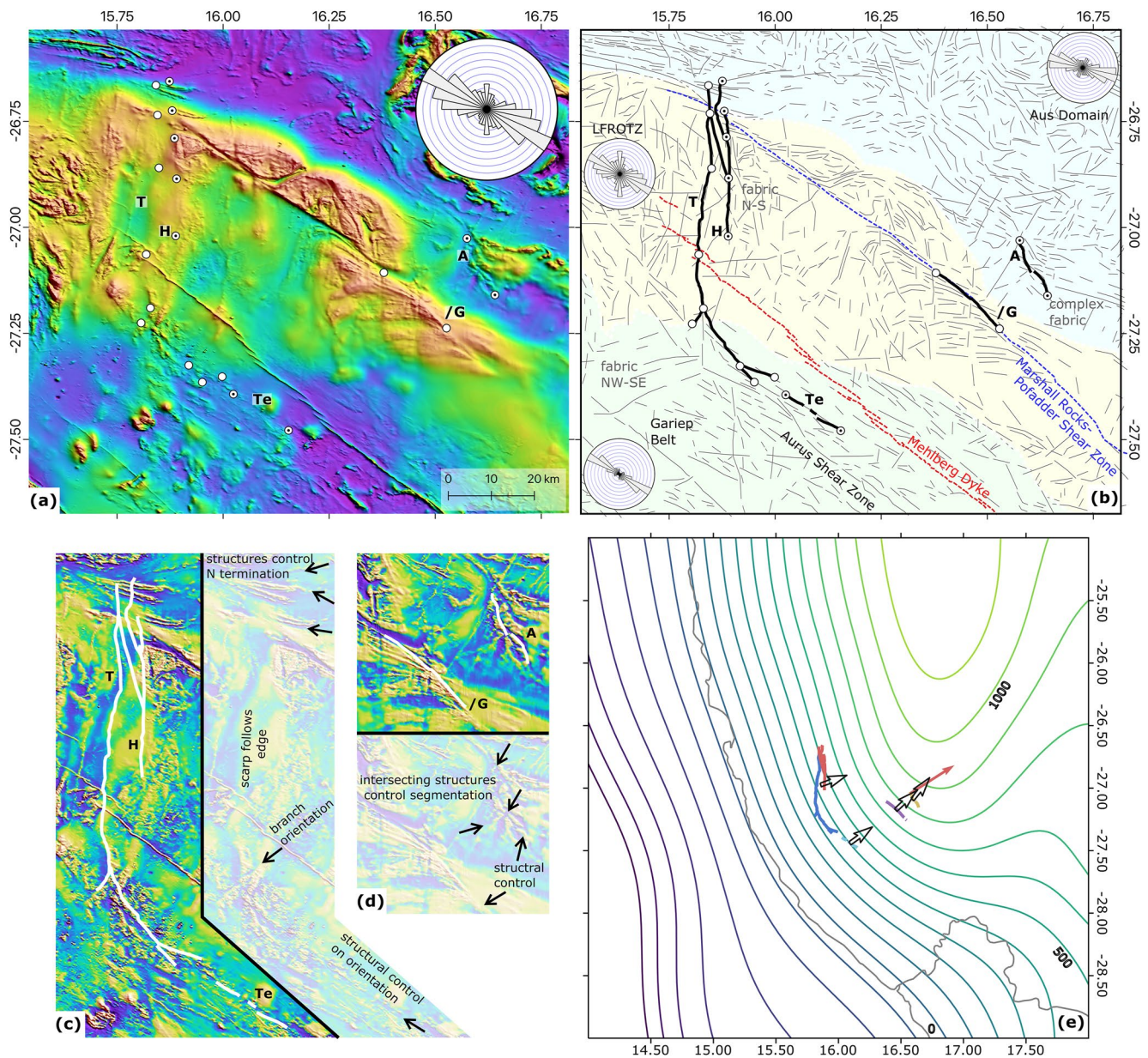


Figure 7. Controls on the slip, orientation and location of fault reactivation. (a) Map of aeromagnetic data (reduced to pole) of the study region, scarps are shown as dots on the aeromagnetic data (which are also shown on (b)). Inset: Rose diagram summarizing the interpreted fabric orientations visible as lineaments in the aeromagnetic data (see (b)) throughout the entire mapped area. (b) Interpretative sketch of the lineaments (gray lines), tectonic domains, and regional features within the Namaqua-Natal and the Gariep belts, based on aeromagnetic data and field mapping (Macey et al., 2022). Inset: rose diagrams summarizing fabric orientations within each tectonic domain. (c and d) Maps of aeromagnetic data (first vertical derivative) and their interpretations alongside, showing details of further structural control on propagation and termination of ruptures. (e) Map of contours of gravitational potential energy (GPE) calculated from smoothed topography (see Figure 1b for topography). White arrows with black outlines point up-slope, in the direction of greatest increase in gravitational potential energy. The red arrow in this panel shows the slip-vector measured for the Anusi-Tafelkop scarp (Figure 6 and Figure S4 in Supporting Information S1). A—Anusi-Tafelkop Fault, /G—/Gâb Fault, H—Hai-s Fault, T—Tsau ||Khaeb Fault, LFRQTZ—Lower-Fish-River Onseepkans Thrust Zone.

5.1. Role of Inherited Structures

The long history of crustal deformation in southern Namibia has influenced the location, orientation and shape of the neotectonic fault traces observed, and likely also influenced the M_{\max} of these structures. Figure 7a shows the location of the recent scarps as dots (compare with Figure 7b) on the aeromagnetic data which have been reduced to the pole (RTP). Initial inspection of the data reveals the presence of at least three magnetic domains which are separated, to first order, by two clear NW-SE striking features. The northern feature corresponds to the

MRPSZ (see interpretation in Figure 7b). This ductile structure initiated at the end of the Namaqua-Orogeny, and has been reactivated to form the /Gäb Fault scarp. The southern feature is the Mehlberg Dyke. The NE domain (Aus Domain) displays a relatively low average magnetic response, dominated by blues and purples, and contains a relatively complex tectonic fabric. This fabric includes a number of curved NW-SE lineaments one of which is closely followed by the Anusi-Tafelkop scarp.

In the central LFROTZ area (Lower-Fish-River-Onseepkans Thrust Zone; Macey et al., 2017), the magnetic response is higher on average (yellows and oranges), but appears to come from variable depths; some areas preserve high frequencies, suggesting a relatively shallow source of the signal whilst other areas show only a low-frequency response, suggesting that the magnetic units are buried deeper beneath non-magnetic cover. Geological mapping identifies the LFROTZ as a wide NE-dipping thrust zone consisting of sheets of high grade metamorphic rocks that were significantly reworked and retrograded during the thrust event. The hydrated retrograde metamorphic mineral assemblages include magnetic minerals such as magnetite (Macey et al., 2022; McDaid, 1978), which may impart the higher magnetic response of this domain. The southern domain (Gariep Belt) has an overall appearance that is similar to the Aus Domain.

More detailed mapping of lithological units and faults was carried out using the first vertical derivative (FVD) of the RTP data (shown in examples in Figures 7c and 7d). The rose diagram in Figure 7a shows the overall orientation of fabric throughout the entire mapped area (see Figure 7b). The dominant orientation is clearly NW-SE, matching the MRPSZ and the Mehlberg Dyke. Interestingly, the /Gäb and Anusi-Tafelkop scarps, as well as the Tsau ||Khaeb extension and the southern portion of the Tsau ||Khaeb scarp follow this dominant structural orientation. The rose diagrams in Figure 7b show the fabric orientations within each of the domains. Although all three domains have a strong WNW-ESE or NW-SE fabric, a N-S fabric dominates locally in the LFROTZ, in exactly the area where the Tsau ||Khaeb scarp runs N-S. As this scarp crosses into the Aurus Shear Zone, its strike changes to follow the clear NW-SE fabric of the shear zone. So it appears that the first order orientations of the recent scarps are strongly controlled by the underlying inherited fabric. The N-S fabric may be related to E-W Gariep Basin rifting, which is also associated with *syn*-rift Gannakouriep ~N-S dykes mapped within the Tsau ||Khaeb (Sperrgebiet) National Park (McDaid, 1978; Reid et al., 1991). These structures are thought to have been reactivated during the Jurassic break-up of Africa and South America, especially along the Luderitz Coast.

Figures 7c and 7d show details of further structural control: the northern termination of the Tsau ||Khaeb scarp co-incides with what appear to be folded units and with a fault that runs ENE-WSW. The minor branch of this scarp (where the scarp turns to follow the Aurus Shear Zone) follows a structural orientation that can be mapped from the FVD and the segmentation of the /Gäb, and Anusi-Tafelkop scarps also seem to be structurally controlled.

5.1.1. Weakening Mechanisms

Studies of both the Aurus Shear Zone and the MRPSZ (sometimes referred to as the Kuckaus Shear Zone in this area) have highlighted the presence of chlorite and muscovite within these shear zones (Diener et al., 2016; Stenvall et al., 2020; Thomas et al., 2016). Stenvall et al. (2020) use $\delta^{18}\text{O}$ values to suggest that these phyllosilicates formed through retrograde reactions associated with the infiltration of at least some fluids of meteoric origin and highlight the contrast with the high-grade anhydrous wall-rocks distal from shear zones. As suggested for other SCR earthquakes, such as the 2016 Petermann Ranges earthquake in Australia (Attanayake et al., 2020), the presence of phyllosilicate minerals may play an important role in facilitating brittle reactivation. The Aus Domain of the Namaqua-Natal Belt, is dominated by anhydrous high-grade metamorphic rocks and appears to lack structures that are prone to brittle reactivation. Contrastingly, the highly retrograded wall-rocks of the ~550 km-long MRPSZ have seen repeated ductile and later brittle reactivation during the complex tectonic history of the region (Macey et al., 2022), and likely represents an exceptionally weakened zone in the crust. Williams, Fagereng, et al. (2022) demonstrate that fault gauge formation and fault zone widening, known to dissipate seismic energy released during an earthquake, is larger where a fault cross-cuts pre-existing fabrics in the southern East African Rift compared with where it parallels it. Since faults in SW Namibia area are so strongly aligned with pre-existing structures and have long-term deformation histories, the expected energy dissipation by these processes is greatly reduced and may contribute to larger M_w earthquakes along these structures.

5.1.2. Regional and Global Comparisons

It is clear that inherited structures control the location, orientation and geometry of faults in Namibia. Further north, E. Salomon et al. (2015) found that steeply dipping coast-parallel ductile structures within the Pan-African

Kaoko Belt were exploited by west-dipping brittle normal faults. Some of these faults offset Etendeka volcanic rocks, deposited shortly before or during the breakup of the South Atlantic, by 400–1,200 m. E. Salomon et al. (2015) attribute this faulting to the opening of the South Atlantic and suggest that the shear zones were reactivated where they were favorably oriented relative to the rifting; though it is difficult to conclusively determine the timing of this faulting. Similarly, G. Salomon et al. (2022) found that the neotectonic Hebron Fault exploited the NNW-SSE Nam shear zone and that the fault was segmented where the ductile structures were interrupted by a granite intrusion.

The close association between Proterozoic orogenic belts and neotectonic brittle deformation has been frequently commented on within the East African Rift (Corti et al., 2007; Craig et al., 2016; Hodge et al., 2018; Ring, 1994; Williams, Fagereng, et al., 2022). Recently, Daly et al. (2020) suggested that the Southwestern Branch of the rift should be viewed as a continuous band of active extension running from the Luangwa rift, through the Okavango Rift and continuing into the Eiseb Rift in NE Namibia. This closely follows the Damara Belt as it passes between the Kalahari and Congo cratons (Corner & Durrheim, 2018). The neotectonic faults within the SW rift are parallel to the ductile Pan-African structures. The results here do not directly discriminate between the various hypotheses proposed for the extension of the south-west branch of the East African Rift beyond the Eiseb Graben (Daly et al., 2020). However, in combination with the Hebron scarp (see G. Salomon et al., 2022), our work suggests that some distributed extension extends along the western margin of the Kalahari Craton following structures within the Gariep and Namaqua-Natal Belts, rather than all of the deformation occurring within the Damara Belt or continuing along the Walvis Ridge.

Recent compilations of reverse-faulting earthquake scarps in Australia also found striking congruence between lineaments in aeromagnetic datasets and recent earthquake ruptures in an SCR setting (King et al., 2019; Yang et al., 2021). In most cases the surface traces of these faults were more complex than those observed here, though Yang et al. (2021) suggest that some ruptures (such as the Petermann earthquake) were relatively straight when there was a single dominant tectonic fabric which was well-aligned to the regional stresses. They found that the more complex ruptures occurred when the dominant fabric was misaligned to the regional stress, or the area is characterized by complex intersecting lineaments.

5.1.3. Driving Stresses

Geological inheritance clearly plays a critical role in the location and orientation of the identified scarps. However, the presence of active normal faulting cannot be explained by structural inheritance. Here we turn to a consideration of the forces arising from the surface slope from the Great Escarpment, the edge of the southern African plateau, down to the coast (Figure 1b). Figure 7e shows contours of GPE from filtered topography. If the plateau were to extend as a result, normal faults would be expected to strike parallel to these contours and perpendicular to the direction of greatest increase in GPE. Intriguingly, the Tsau || Khaeb scarp plots where the orientation of the contours change, perhaps adding a further explanation for slip along pre-existing N-S and NW-SE structures in this area. The red arrow in this panel shows the slip-vector measured for the Anusi-Tafelkop scarp which is consistent with the direction of increasing GPE.

This area has undergone a complex series of deformation events with different orientations (Section 3, Figure 7) and it appears that reactivation may particularly occur on structures well-oriented with respect to the extensional body forces. This alignment may also help to explain the comparatively simple geometry of the faults (as described by Yang et al. (2021) in Australia).

If the gradients of gravitational energy in the region do drive deformation along the edge of the Great Escarpment, then rather than seismic hazard being solely associated with the East African Rift and its extensions, major normal faulting events may occur more broadly where orogenic belts align with extensional stresses associated with the anomalously high elevation of the Southern African Plateau. An alternative or complementary mechanism that could promote seismicity in this region is the unloading associated with the erosional retreat of the Great Escarpment, although the overwhelming majority of the erosion associated with the escarpment retreat occurred in the Cretaceous, perhaps with a significant delay in, or prolonged, tectonic response (Brown et al., 1990; Raab et al., 2005; Wildman et al., 2021). Paleogene volcanism may also have played a role in the timing and location of faulting. The eruption of carbonatites in the region, particularly of Dicker Willem (Figure 1b), may have caused localized thermally induced uplift and weakening of ductile shear zones at depth. This may have induced the vertical stress required to drive rupture and further weakened the crust along older

structures. However, it remains unclear whether there was significant uplift associated with this volcanism and whether brittle deformation would have facilitated it (Walter et al., 2022). While the dynamics and timing of brittle deformation in SW Namibia remain in question and require the collection of additional time-calibrated structural data, it seems likely that body stresses associated with the gravitational energy contrasts caused by the plateau drive the observed extensional deformation. These stresses may be modified by variations in ridge-push associated with changing spreading rates of the Mid-Atlantic Ridge (Dauteuil et al., 2018; Müller et al., 2008) and/or the effects of volcanism.

The /Gāb and Anusi-Tafelkop faults both have up-hill (northwest) facing scarps. This is compatible with the proposed gravitational control on extension. For instance uphill-facing scarps are typical of sackungen, which are thought to be caused by gravitational spreading on steep ridges Radbruch-Hall (1978). On a larger scale normal faults perpendicular to gradients of GPE take up horizontal extension and vertical thinning regardless of their dip direction. The fact that these normal fault scarps face the higher topography may appear unusual to workers from more rapidly deforming regions as in such areas the relief is primarily controlled by the cumulative fault displacement. This results in higher topography associated with normal fault footwalls and downhill-facing scarps. In the study area the relief is primarily controlled by the formation of the Great Escarpment, likely through deep-seated isostatic or dynamic uplift, and subsequent erosion. The limited cumulative offset on the Anusi-Tafelkop fault indicates that faulting plays only a limited second-order role in controlling the topography. Future studies attempting to locate similar features should take this decoupling of fault dip from the large-scale topography into account.

5.2. Comparison With Previous Local Studies of Neotectonics

Dauteuil et al. (2018) interpret surface microstructures in the coastal Tsau ||Khaeb National Park (Sperrgebiet) as tectonic in origin. By measuring the orientations of striations and joints within Oligo-Miocene deposits, they conclude that there are two periods of regional brittle deformation: An initial WNW-ESE extension followed by rotated NE-SW extension. Our results are broadly compatible with extension in these directions, however, many of the microstructures Dauteuil et al. (2018) describe record cm-scale pure strike slip motion, which are dissimilar to the much larger-scale predominantly DS structures described here. The microstructures studied by Dauteuil et al. (2018) are assigned a maximum age of early Miocene, and this is compatible with the scarcely available chronologic information used to constrain the fault scarps in this study. Elsewhere in southern Namibia at the Fish River Canyon, Mvondo et al. (2011) infer Plio-Pleistocene NW-SE extension on NE-SW orientated grabens, but the timing of this deformation is not well constrained. In order to establish a robust Cenozoic tectonic history of southern Namibia, more detailed time-calibrated paleoseismic studies on recently active fault scarps are required.

5.3. Reactivation in Single or Multiple Events?

Calais et al. (2016) proposed that SCR earthquakes may generally release ancient strain reservoirs and be triggered by transient changes in stress and/or fault stress. This model predicts that SCR events may be spatially and temporally clustered (due to stress interactions between faults) but that it would be expected individual faults would be extremely slow to reload and have a repeat event due to a very slow secular loading rate. In some cases the earthquakes may release “fossil” strain reservoirs accumulated during a former stress regime with very different characteristics to that found in the present day (Craig et al., 2016). In such cases events would not necessarily be expected to repeat on the same structure at all. Calais et al. (2016) highlighted the Hebron Fault scarp in Namibia as an example of a scarp that apparently formed in a single event to support this model. Subsequent detailed geomorphological analyses failed to find evidence of a multiple-event origin but noted that this implied an extreme slip-to-length ratio if the single event hypothesis were correct (G. Salomon et al., 2022). In contrast, here observations of compound scarps, abrupt changes in scarp height between geomorphological surfaces of contrasting age and fault scaling relationships suggest that the Tsau ||Khaeb, Hai-s and/Gāb all formed in two or more events. The model of Calais et al. (2016) poses great problems for probabilistic seismic hazard assessment in SCRs. If hazard moves between fault systems, releasing ancient strain reservoirs, it is very difficult to identify possible sources of future hazard based on historical or even paleoseismic events. It is widely recognized that instrumental catalogs are insufficient to identify which areas may experience large magnitude seismicity in the future in areas which are very slowly deforming and the return time of major earthquakes could be 100 ka or more. Extended aftershock sequences in such regions may dominate the recent record of moderate-magnitude

seismicity and not represent the average distribution of seismicity over multiple earthquake cycles (Stein & Liu, 2009). Incorporating information from neotectonic faults is one way of ameliorating this deficiency, but this is only possible if earthquakes are expected to reoccur on individual structures on timescales short enough for evidence of the previous event to be visible. These faults suggest that this is the case for at least some major faults in Namibia.

5.4. Geometry and M_{\max}

Even accounting for the evidence that the scarps formed in multiple events they appear likely to have formed in remarkably large earthquakes. If we assume that the entire length of the Anusi-Tafelkop scarp last failed in a single event, and that the Tsau ||Khaeb Fault has undergone segmented rupture we obtain a range in expected moment magnitude 6.3–7.2. M_w 7.2 events lie at the upper end of normal faulting earthquakes observed during the instrumental period (Neely & Stein, 2021) and the inferred magnitudes lie well above the maximum magnitude recorded in the instrumental record within Namibia (M_w 5.5). The presence of such large events should thus be considered when estimating M_{\max} for the purposes of probabilistic seismic hazard analysis, especially as M_{\max} estimated from catalog data tends to be much lower within the region (e.g., Midzi et al., 2020). It seems likely that the relatively large magnitude estimates are connected to the fact that the faults reactivate major strike-slip shear zones. The scarps have remarkably straight simple geometries when compared to many continental normal faults (Biasi & Wesnousky, 2017). The presence of a straight preexisting weaknesses may allow a geometrically simple major normal fault zone to establish quickly in comparison to a fault zone forming through the linkage of smaller individual parallel normal faults distributed relatively randomly throughout the region (Cowie et al., 2000). As discussed above, near optimal alignment between the strong regional tectonic fabric and the potential driving stresses may also contribute to the development of long straight faults. The possibility of relatively large earthquakes on these and similar structures should be incorporated into fault source models for use in seismic hazard assessments.

5.5. Total Offset

By measuring the approximate elevation differences between sub-horizontal beds within the Nama Group, and the non-conformity at the base of it at Hill B, 20 m displacement across the Anusi-Tafelkop Fault is calculated (Figure S5 in Supporting Information S1). Since there is no simple way to determine when the bulk of this displacement occurred, this displacement represents that accumulated since Ediacaran-Cambrian deposition of the Nama Group, including the 1.2 m within recent alluvium. Considering the scarp in this area is 15 km long, 20 m cumulative offset is surprisingly small, and illustrates that significant seismicity can be produced from structures that have only accumulated minor prior displacement. Similar under-displacement is also observed for the Hebron Fault (G. Salomon et al., 2022), which also offsets the Nama Group, and other normal faults in relatively slowly deforming regions (Walker et al., 2017). This feature of the faults in this region increases the difficulty of confidently identifying faults capable of significant neotectonic rupture in areas with less exceptional geomorphological preservation.

5.6. Implications of Apparent Clustering

The identification of a cluster of major fault scarps in a fairly small area could be interpreted as evidence that this area may be deforming more rapidly than other parts of Namibia and southern Africa. Studies in Australia and north China have found evidence for clustering and migration of SCR seismicity whereby a group of faults experiences a concentrated period of deformation before becoming inactive and the locus of seismicity shifts to another fault system (Clark et al., 2012; Liu et al., 2011), and it is possible that a similar process may occur in our study area.

It is however important to note the exceptional preservation potential associated with the lack of anthropogenic activity, aridity and widespread concretization of low relief geomorphological surfaces. It is very likely that such features would be effectively disguised (or at least their tectonic origin would become ambiguous) in areas with higher rates of erosion due to climate, agriculture, or different soil characteristics. Further into the interior of Namibia many faults can be identified displacing the Nama Group, but the lack of a veneer of recent cover capable of preserving a scarp for kyr timescales prevent us from being able to state whether these faults have

been active on neotectonic timescales. The instrumental catalog does record more moderate-magnitude seismicity between the coast and the Great Escarpment, however, only two events are within the study area (Figures 1a and 1b).

Given these uncertainties it is safer to view this region as a window into long term neotectonic processes which may also occur elsewhere in the region, and to view it as an area of exceptional preservation rather than exceptional activity. This suggests that in other areas, which are less arid or which lack calcretized sediments capable of preserving the signature of earthquake surface ruptures, it may be necessary to include analogous structures which are well-oriented with respect to the present-day stress field, but which lack obvious signs of neotectonic rupture, as possible sources of hazard. This is especially true when conducting hazard assessments for critical infrastructure such as nuclear power stations (as is currently being undertaken in South Africa).

The incorporation of fault source models into probabilistic seismic hazard models in comparatively slowly deforming regions has been undertaken in Australia (Allen et al., 2018; Clark et al., 2016) and, within the region, in Malawi (Hodge et al., 2015; Wedmore et al., 2020; Williams, Wedmore, et al., 2022). Hodge et al. (2015) demonstrated that this approach can significantly affect model outcomes, and this is especially true in slowly deforming areas with limited instrumental records. In an under-studied and slowly deforming region such as Namibia the same is likely to be true, but uncertainties on such estimates will remain high until bounds can be placed on fault slip rates through more detailed paleoseismic and geodetic studies.

6. Conclusion

Remote sensing, field observations and GPS profiles confirm four new fault scarps in southern Namibia that represent a number of M_w 6.4– M_w 7.2 earthquakes. These, and events associated with the Hebron Fault scarp, are substantially larger than the largest event in the instrumental seismic record ($\sim M_w$ 5.4) of Namibia and indicate that large earthquakes can and have occurred. The presence of these structures in a region with a limited record of instrumental seismicity suggests that the M_{max} of this area may be much larger than previously assumed. This highlights the necessity of incorporating information from fault studies into probabilistic seismic hazard assessments in this region, in a similar way to other SCRs such as Australia. The fact that such major structures have gone hitherto unrecorded suggests significant further research is needed to characterize these sources of hazard.

We demonstrate that pre-existing structures control the location and orientation of fault scarps, and that reactivation occurs where such structures are well-oriented with respect to stresses arising from the gradients in GPE. Furthermore, it appears that the local GPE controls the slip vector along the faults. The well-developed nature of the ancient weaknesses that are reactivated by the faults means that large earthquakes can be generated where there is limited cumulative offset, making it difficult to rule out features that are not considered potentially hazardous.

It should be noted that the area studied is ideally suited to identifying such events due to its hyper-aridity, slow erosion rates, and because sediments are extensively cemented and strengthened by secondary calcium carbonates. Where these features are not present, such a prolonged record of events is unlikely to be preserved, generating biases that must be accounted for in future seismic hazard models.

Data Availability Statement

Pléiades images (© Centre national d'études spatial - CNES, 2021; distribution Airbus) were purchased via the DINAMIS platform (<https://dinamis.data-terra.org/en/homepage/>). Other imagery was accessed through Bing Maps (<https://www.bing.com/maps>). Real Time Kinematic GPS Displacement profiles are available through Ziva-Hub (<https://doi.org/10.25375/uct.21666482>). Aeromagnetic data and geological maps are available for purchase from the Geological Survey of Namibia on request (<https://www.mme.gov.na/gsn/services/>).

References

- Allen, T. I., Griffin, J., Ghasemi, H., Leonard, M., & Clark, D. (2018). The 2018 National Seismic Hazard Assessment for Australia: Model overview.
- Allen, T. I., Griffin, J. D., Leonard, M., Clark, D. J., & Ghasemi, H. (2020). The 2018 National Seismic Hazard Assessment of Australia: Quantifying hazard changes and model uncertainties. *Earthquake Spectra*, 36(1_suppl), 5–43. <https://doi.org/10.1177/8755293019900777>

Acknowledgments

Jessica Gaingos is thanked for providing accurate pronunciations of the Khoekhoegowab words /Gāb, Hai-s, and Tsau ||Khaeb. Tamarah King and Luke Wedmore are thanked for thoughtful reviews which greatly improved the manuscript. Landowners are thanked for access to farm land and the Namibian National Parks for permission to access into the Tsau ||Khaeb National Park (Sperrgebiet). The Namibian Geological Survey and South African Council for Geoscience are thanked for their invitation to participate in the research trip, their support while in the field and access to geological and geophysical data. Thanks are extended to Shane Doggart for his role in identifying the Anusi-Tafelkop Fault and to Roshan Klein for assisting with fieldwork. RAM and VLS were funded by the Claude Leon Foundation and RAS acknowledges financial support from the National Research Foundation of South Africa (NRF Grants 118831 and 110780). Pléiades satellite images were acquired by JH and RAS via the DINAMIS platform (project: 2021-092-Sci).

- Attanayake, J., King, T. R., Quigley, M. C., Gibson, G., Clark, D., Jones, A., et al. (2020). Rupture characteristics and bedrock structural control of the 2016 Mw 6.0 intraplate earthquake in the Petermann Ranges, Australia. *Bulletin of the Seismological Society of America*, 110(3), 1037–1045. <https://doi.org/10.1785/0120190266>
- Biasi, G. P., & Wesnousky, S. G. (2017). Bends and ends of surface ruptures. *Bulletin of the Seismological Society of America*, 107(6), 2543–2560. <https://doi.org/10.1785/0120160292>
- Bierman, P. R., & Caffee, M. (2001). Slow rates of rock surface erosion and sediment production across the Namib Desert and escarpment, southern Africa. *American Journal of Science*, 301(4–5), 326–358. <https://doi.org/10.2475/ajs.301.4-5.326>
- Birkeland, P. W. (1984). *Soils and geomorphology*. Oxford University Press.
- Brown, R. W., Rust, D. J., Summerfield, M. A., Gleadow, A. J. W., & Wit, M. C. J. D. (1990). An Early Cretaceous phase of accelerated erosion on the south-western margin of Africa: Evidence from apatite fission track analysis and the offshore sedimentary record. *International Journal of Radiation Applications and Instrumentation*, 17(3), 339–350. [https://doi.org/10.1016/1359-0189\(90\)90056-4](https://doi.org/10.1016/1359-0189(90)90056-4)
- Calais, E., Camelbeeck, T., Stein, S., Liu, M., & Craig, T. J. (2016). A new paradigm for large earthquakes in stable continental plate interiors. *Geophysical Research Letters*, 43, 10621–10637. <https://doi.org/10.1002/2016GL070815>
- Clark, D., Leonard, M., Griffin, J., Stirling, M., & Volti, T. (2016). Incorporating fault sources into the Australian National Seismic Hazard Assessment (NSHA) 2018. In *Australian Earthquake Engineering Society 2016 Conference*.
- Clark, D., McPherson, A., & Van Dissen, R. (2012). Long-term behaviour of Australian stable continental region (SCR) faults. *Tectonophysics*, 566, 1–30. <https://doi.org/10.1016/j.tecto.2012.07.004>
- Cockburn, H., Brown, R., Summerfield, M., & Seidl, M. (2000). Quantifying passive margin denudation and landscape development using a combined fission-track thermochronology and cosmogenic isotope analysis approach. *Earth and Planetary Science Letters*, 179(3–4), 429–435. [https://doi.org/10.1016/S0012-821X\(00\)00144-8](https://doi.org/10.1016/S0012-821X(00)00144-8)
- Corner, B. (2000). Crustal framework of Namibia derived from magnetic and gravity data. *Communications of the Geological Survey of Namibia*, 12, 13–19.
- Corner, B., & Durrheim, R. J. (2018). An integrated geophysical and geological interpretation of the southern African lithosphere. In *Geology of southwest Gondwana* (pp. 19–61). Springer.
- Corti, G., van Wijk, J., Cloetingh, S., & Morley, C. K. (2007). Tectonic inheritance and continental rift architecture: Numerical and analogue models of the East African Rift system. *Tectonics*, 26(6). <https://doi.org/10.1029/2006tc002086>
- Cowie, P., Gupta, S., & Dawers, N. (2000). Implications of fault array evolution for synrift depocentre development: Insights from a numerical fault growth model. *Basin Research*, 12(3–4), 241–261. <https://doi.org/10.1111/j.1365-2117.2000.00126.x>
- Craig, T., Calais, E., Fleitout, L., Bollinger, L., & Scotti, O. (2016). Evidence for the release of long-term tectonic strain stored in continental interiors through intraplate earthquakes. *Geophysical Research Letters*, 43(13), 6826–6836. <https://doi.org/10.1002/2016glo69359>
- Daly, M. (1988). Crustal shear zones in central Africa: A kinematic approach to Proterozoic tectonics. *Episodes Journal of International Geoscience*, 11(1), 5–11. <https://doi.org/10.18814/epiuiugs/1988/v11i1/003>
- Daly, M., Green, P., Watts, A., Davies, O., Chibesakunda, F., & Walker, R. (2020). Tectonics and landscape of the central African Plateau and their implications for a propagating Southwestern Rift in Africa. *Geochemistry, Geophysics, Geosystems*, 21(6), e2019GC008746. <https://doi.org/10.1029/2019gc008746>
- Dauteuil, O., Picart, C., Guillocheau, F., Pickford, M., & Senut, B. (2018). Cenozoic deformation and geomorphic evolution of the Sperrgebiet (southern Namibia). *Communications of the Geological Survey of Namibia*, 18, 1–18.
- Diener, J. F., Fagereng, Å., & Thomas, S. A. (2016). Mid-crustal shear zone development under retrograde conditions: Pressure–temperature–fluid constraints from the Kuckaus Mylonite Zone, Namibia. *Solid Earth*, 7(5), 1331–1347. <https://doi.org/10.5194/se-7-1331-2016>
- Dingle, R. V., Siesser, W. G., & Newton, A. R. (1983). *Mesozoic and tertiary geology of southern Africa*. AA Balkema.
- Frimmel, H. (2008). The Gariep belt. In R. Miller (Ed.), *The geology of Namibia* (pp. 14–39). Geological Survey of Namibia.
- Hasterok, D., Halpin, J. A., Collins, A. S., Hand, M., Kreemer, C., Gard, M. G., & Glorie, S. (2022). New maps of global geological provinces and tectonic plates. *Earth-Science Reviews*, 231, 104069. <https://doi.org/10.1016/j.earscirev.2022.104069>
- Hodge, M., Biggs, J., Goda, K., & Aspinall, W. (2015). Assessing infrequent large earthquakes using geomorphology and geodesy: The Malawi rift. *Natural Hazards*, 76(3), 1781–1806. <https://doi.org/10.1007/s11069-014-1572-y>
- Hodge, M., Fagereng, Å., Biggs, J., & Mdala, H. (2018). Controls on early-rift geometry: New perspectives from the Bilila-Mtakataka Fault, Malawi. *Geophysical Research Letters*, 45(9), 3896–3905. <https://doi.org/10.1029/2018gl077343>
- ISC (2022). On-line Bulletin. <https://doi.org/10.31905/D808B830>
- Johansson, Å., Bingen, B., Huhma, H., Waight, T., Vestergaard, R., Soesoo, A., et al. (2022). A geochronological review of magmatism along the external margin of Columbia and in the Grenville-age orogens forming the core of Rodinia. *Precambrian Research*, 371, 106463. <https://doi.org/10.1016/j.precamres.2021.106463>
- Johnson, K. L., Nissen, E., & Lajoie, L. (2018). Surface rupture morphology and vertical slip distribution of the 1959 M w 7.2 Hebgen Lake (Montana) earthquake from airborne lidar topography. *Journal of Geophysical Research: Solid Earth*, 123(9), 8229–8248. <https://doi.org/10.1029/2017jb015039>
- Johnson, M., Van Vuuren, C., Hegenberger, W., Key, R., & Show, U. (1996). Stratigraphy of the karoo supergroup in southern Africa: An overview. *Journal of African Earth Sciences*, 23(1), 3–15. [https://doi.org/10.1016/s0899-5362\(96\)00048-6](https://doi.org/10.1016/s0899-5362(96)00048-6)
- King, T. R., Quigley, M., & Clark, D. (2019). Surface-rupturing historical earthquakes in Australia and their environmental effects: New insights from re-analyses of observational data. *Geosciences*, 9(10), 408. <https://doi.org/10.3390/geosciences9100408>
- Kolawole, F., Atekwana, E. A., Laó-Dávila, D. A., Abdelsalam, M., Chindandali, P., Salima, J., & Kalindekafa, L. (2018). Active deformation of Malawi rift's north basin Hinge zone modulated by reactivation of preexisting Precambrian shear zone fabric. *Tectonics*, 37(3), 683–704. <https://doi.org/10.1002/2017tc004628>
- Leonard, M. (2014). Self-consistent earthquake fault-scaling relations: Update and extension to stable continental strike-slip faults. *Bulletin of the Seismological Society of America*, 104(6), 2953–2965. <https://doi.org/10.1785/0120140087>
- Liu, M., Stein, S., & Wang, H. (2011). 2000 years of migrating earthquakes in North China: How earthquakes in midcontinents differ from those at plate boundaries. *Lithosphere*, 3(2), 128–132. <https://doi.org/10.1130/l129.1>
- Macey, P. H., Thomas, R., Kisters, A., Diener, J., Angombe, M., & Deggart, S. (2022). A continental back-arc setting for the Namaqua belt: Evidence from the Kakamas domain. *Geoscience Frontiers*, 101408.
- Macey, P. H., Thomas, R. J., Minnaar, H. M., Gresse, P. G., Lambert, C. W., Groenewald, C. A., et al. (2017). Origin and evolution of the ~1.9 Ga Richtersveld magmatic Arc, SW Africa. *Precambrian Research*, 292, 417–451. <https://doi.org/10.1016/j.precamres.2017.01.013>
- Marsh, J. (1975). The Lüderitz Alkaline Province, South West Africa I: Descriptive petrology of the Granitberg Foyaité complex. *South African Journal of Geology*, 78(2), 215–224.

- Marsh, J., Phillips, D., & Lock, B. (2010). 40Ar/39Ar dating of the Klinghardt and Stalhart Phonolites, Namibia, and comments on the evolution of the Klinghardt volcanic field. *Communications of the Geological Survey of Namibia*, 20, 1–8.
- McDaid, J. M. (1978). The geology of the northern part of diamond area no 1., south west Africa. In *14th and 15th Annual Reports of the Precambrian Research Unit* (pp. 124–140).
- Midzi, V., Manzunzu, B., Mulabisana, T., Zulu, B., Pule, T., & Myendeki, S. (2020). Probabilistic seismic hazard maps for South Africa. *Journal of African Earth Sciences*, 162, 103689. <https://doi.org/10.1016/j.jafrearsci.2019.103689>
- Miller, R. M., Krapf, C., Hoey, T., Fitchett, J., Nguno, A. K., Muyambas, R., et al. (2021). A sedimentological record of fluvial-aeolian interactions and climate variability in the hyperarid northern namib desert, Namibia. *South African Journal of Geology*, 124(3), 575–610. <https://doi.org/10.25131/sajg.124.0008>
- Müller, R. D., Sdrolias, M., Gaina, C., & Roest, W. R. (2008). Age, spreading rates, and spreading asymmetry of the world's ocean crust. *Geochemistry, Geophysics, Geosystems*, 9(4). <https://doi.org/10.1029/2007gc001743>
- Mvondo, F., Dauteuil, O., & Guillocheau, F. (2011). The Fish River Canyon (Southern Namibia): A record of Cenozoic mantle dynamics? *Comptes Rendus Geoscience*, 343(7), 478–485. <https://doi.org/10.1016/j.crte.2011.07.003>
- NASA/JPL. (2013). NASA Shuttle Radar Topography Mission Global 1 arc second. Last accessed 25 May 2021. <https://doi.org/10.5067/MEaSUREs/SRTM/SRTMGL1.003>
- Neely, J. S., & Stein, S. (2021). Why do continental normal fault earthquakes have smaller maximum magnitudes? *Tectonophysics*, 809, 228854. <https://doi.org/10.1016/j.tecto.2021.228854>
- Picart, C., Dauteuil, O., Pickford, M., & Owono, F. M. (2020). Cenozoic deformation of the South African plateau, Namibia: Insights from planation surfaces. *Geomorphology*, 350, 106922. <https://doi.org/10.1016/j.geomorph.2019.106922>
- Pickford, M. (2015). Cenozoic geology of the Northern Sperrgebiet, Namibia, accenting the Palaeogene. *Communications of the Geological Survey of Namibia*, 16, 10–104.
- Pickford, M., Senut, B., Morales, J., & Sanchez, I. (2008). *Fossiliferous Cainozoic carbonates of the northern Sperrgebiet* (Vol. 20, pp. 25–42). Memoir of the Geological Survey of Namibia.
- Raab, M. J., Brown, R. W., Gallagher, K., Weber, K., & Gleadow, A. J. (2005). Denudational and thermal history of the Early Cretaceous Brandberg and Okenyenya igneous complexes on Namibia's Atlantic passive margin. *Tectonics*, 24(3), 1–15. <https://doi.org/10.1029/2004TC001688>
- Radbruch-Hall, D. H. (1978). Gravitational creep of rock masses on slopes. *Developments in Geotechnical Engineering*, (Vol. 14, pp. 607–657). Elsevier.
- Reid, D., Ransome, I., Onstott, T., & Adams, C. (1991). Time of emplacement and metamorphism of Late Precambrian mafic dykes associated with the Pan-African Gariep orogeny, Southern Africa: Implications for the age of the Nama Group. *Journal of African Earth Sciences (and the Middle East)*, 13(3–4), 531–541. [https://doi.org/10.1016/0899-5362\(91\)90116-G](https://doi.org/10.1016/0899-5362(91)90116-G)
- Reid, D., & Rex, D. (1994). Cretaceous dykes associated with the opening of the South Atlantic: The Mehlberg dyke, northern Richtersveld. *South African Journal of Geology*, 97(2), 135–165.
- Ring, U. (1994). The influence of preexisting structure on the evolution of the Cenozoic Malawi rift (East African rift system). *Tectonics*, 13(2), 313–326. <https://doi.org/10.1029/93tc03188>
- Rioux, M., Bowring, S., Dudás, F., & Hanson, R. (2010). Characterizing the U–Pb systematics of baddeleyite through chemical abrasion: Application of multi-step digestion methods to baddeleyite geochronology. *Contributions to Mineralogy and Petrology*, 160(5), 777–801. <https://doi.org/10.1007/s00410-010-0507-1>
- Salomon, E., Koehn, D., & Passchier, C. (2015). Brittle reactivation of ductile shear zones in NW Namibia in relation to South Atlantic rifting. *Tectonics*, 34(1), 70–85. <https://doi.org/10.1002/2014tc003728>
- Salomon, G., New, T., Muir, R., Whitehead, B., Scheiber-Enslin, S., Smit, J., et al. (2022). Geomorphological and geophysical analyses of the Hebron Fault, SW Namibia: Implications for stable continental region seismic hazard. *Geophysical Journal International*, 229(1), 235–254. <https://doi.org/10.1093/gji/ggab466>
- Stein, S., & Liu, M. (2009). Long aftershock sequences within continents and implications for earthquake hazard assessment. *Nature*, 462(7269), 87–89. <https://doi.org/10.1038/nature08502>
- Stenvall, C., Fagereng, A., Diener, J., Harris, C., & Janney, P. (2020). *Sources and effects of fluids in continental retrograde shear zones: Insights from the Kuckaus Mylonite zone*. Namibia.
- Stirling, M., Rhoades, D., & Berryman, K. (2002). Comparison of earthquake scaling relations derived from data of the instrumental and preinstrumental era. *Bulletin of the Seismological Society of America*, 92(2), 812–830. <https://doi.org/10.1785/0120000221>
- Thomas, R. J., Macey, P. H., Spencer, C., Dhansay, T., Diener, J. F., Lambert, C. W., et al. (2016). The Sperrgebiet domain, Aurus mountains, SW Namibia: A ~2020–850 Ma window within the Pan-African Gariep orogen. *Precambrian Research*, 286, 35–58. <https://doi.org/10.1016/j.precamres.2016.09.023>
- Thompson, S. C., Weldon, R. J., Rubin, C. M., Abdrakhmatov, K., Molnar, P., & Berger, G. W. (2002). Late Quaternary slip rates across the central Tien Shan, Kyrgyzstan, central Asia. *Journal of Geophysical Research*, 107(B9), ETG7-1–ETG7-32. <https://doi.org/10.1029/2001jb000596>
- Torsvik, T. H., & Cocks, L. R. M. (2013). Gondwana from top to base in space and time. *Gondwana Research*, 24(3–4), 999–1030. <https://doi.org/10.1016/j.gr.2013.06.012>
- Viola, G., Andreoli, M., Ben-Avraham, Z., Stengel, I., & Reshef, M. (2005). Offshore mud volcanoes and onland faulting in southwestern Africa: Neotectonic implications and constraints on the regional stress field. *Earth and Planetary Science Letters*, 231(1–2), 147–160. <https://doi.org/10.1016/j.epsl.2004.12.001>
- Walker, R., Wegmann, K., Bayasgalan, A., Carson, R., Elliott, J., Fox, M., et al. (2017). The Egiin Davaa prehistoric rupture, central Mongolia: A large magnitude normal faulting earthquake on a reactivated fault with little cumulative slip located in a slowly deforming intraplate setting. *Seismicity, fault rupture and earthquake hazards in slowly deforming regions*, (Vol. 432, pp. 187–212). Geological Society of London.
- Walter, B. F., Giebel, J., Marlow, A. G., Siegfried, P. R., Marks, M., Markl, G., et al. (2022). The Kieshöhe carbonatites of southwestern Namibia—the post-magmatic role of silicate xenoliths on REE mobilisation. *Communications of the Geological Survey of Namibia*, 25, 1–31.
- Wanke, H. (2005). The Namibian Eiseb Graben as an extension of the East African rift: Evidence from Landsat TM 5 imagery. *South African Journal of Geology*, 108(4), 541–546. <https://doi.org/10.2113/108.4.541>
- Ward, J., Seely, M., & Lancaster, N. (1983). On the antiquity of the Namib. *South African Journal of Science*, 79(5), 175–183.
- Wedmore, L., Biggs, J., Floyd, M., Fagereng, Å., Mdala, H., Chindandali, P., et al. (2021). Geodetic constraints on cratonic microplates and broad strain during rifting of thick Southern African lithosphere. *Geophysical Research Letters*, 48(17), e2021GL093785. <https://doi.org/10.1029/2021gl093785>
- Wedmore, L., Biggs, J., Williams, J., Fagereng, Å., Dulanya, Z., Mphepo, F., & Mdala, H. (2020). Active fault scarps in southern Malawi and their implications for the distribution of strain in incipient continental rifts. *Tectonics*, 39(3), e2019TC005834. <https://doi.org/10.1029/2019tc005834>

- Wedmore, L., Turner, T., Biggs, J., Williams, J. N., Sickingabula, H. M., Kabumbu, C., & Banda, K. (2022). The Luangwa rift active fault database and fault reactivation along the southwestern branch of the East African Rift. *Solid Earth*, 13(11), 1731–1753. <https://doi.org/10.5194/se-13-1731-2022>
- Wells, D. L., & Coppersmith, K. J. (1994). New empirical relationships among magnitude, rupture length, rupture width, rupture area, and surface displacement. *Bulletin of the Seismological Society of America*, 84(4), 974–1002.
- White, S., Stollhofen, H., Stanistreet, I. G., & Lorenz, V. (2009). Pleistocene to recent rejuvenation of the Hebron fault, SW Namibia. *Palaeoseismology: Historical and prehistorical records of earthquake ground effects for seismic hazard assessment*, 316(1), 293–317. <https://doi.org/10.1144/SP316.18>
- Wildman, M., Gallagher, K., Chew, D., & Carter, A. (2021). From sink to source: Using offshore thermochronometric data to extract onshore erosion signals in Namibia. *Basin Research*, 33(2), 1580–1602. <https://doi.org/10.1111/bre.12527>
- Williams, J. N., Fagereng, Å., Wedmore, L. N., Biggs, J., Mdala, H., Mphepo, F., & Hodge, M. (2022). Low dissipation of earthquake energy where a fault follows pre-existing weaknesses: Field and microstructural observations of Malawi's Bilila-Mtakataka Fault. *Geophysical Research Letters*, 49(8), e2021GL095286. <https://doi.org/10.1029/2021gl095286>
- Williams, J. N., Wedmore, L. N., Scholz, C. A., Kolawole, F., Wright, L. J., Shillington, D. J., et al. (2022). The Malawi Active Fault Database: An onshore-offshore database for regional assessment of seismic hazard and tectonic evolution. *Geochemistry, Geophysics, Geosystems*, 23(5), e2022GC010425. <https://doi.org/10.1029/2022gc010425>
- Yang, H., Quigley, M., & King, T. (2021). Surface slip distributions and geometric complexity of intraplate reverse-faulting earthquakes. *GSA Bulletin*, 133(9–10), 1909–1929. <https://doi.org/10.1130/B35809.1>